Forside

Eksamensinformation
NFYK10020E - Physics Thesis 60 ECTS, Niels Bohr Institute - Kontrakt:134135 (Oliver Holmegaard Schwarze)

Besvarelsen afleveres af
Oliver Holmegaard Schwarze
ksh820@alumni.ku.dk

Eksamensadministratorer
Eksamensteam, tel 35 33 64 57
eksamen@science.ku.dk

Bedømmere
Karsten Flensberg
Eksaminator
flensberg@nbi.ku.dk
+4535320418

Besvarelsesinformationer

Titel: Finite Element Modeling of Germanium Spin Devices
Titel, engelsk: Finite Element Modeling of Germanium Spin Devices
Tro og love-erklæring: Ja
Indeholder besvarelsen fortroligt materiale: Nej

UNIVERSITY OF COPENHAGEN
FACULTY OF SCIENCE

Master Thesis

Finite Element Modeling of Germanium Spin Devices

Oliver Holmegaard Schwarze

Advisor: Karsten Flensberg

Submitted: May 21, 2023

Abstract

Hole spin-qubits in Germanium are an emerging new platform for developing robust and scalable quantum computers. Main advantages of this platform include fast and accurate addressing of the spins using electrostatic gates, as well as the possibility of interactions of the spin qubits with superconductors. In this project, we develop a computational method for accurately modeling spin-qubits in Germanium and their coupling via a superconductor. Based on the $k \cdot p$ model and the theory of invariants, we construct an envelope-function Hamiltonian for describing hole states in Germanium heterostructures. Using the finite element method, we determine eigenstates of this Hamiltonian, and using these we show that it is possible to make the qubit robust towards gate noise by selecting specific directions of the external magnetic field. We also demonstrate how to determine the coupling strength of two quantum dots connected via a superconductor, and how to tune this coupling strength via the chemical potential in the superconductor. Lastly, we study the minimal Kitaev chain and how to tune the system such that it can host poor man's Majorana states.

Acknowledgements

I would like to thank my supervisor, Karsten Flensberg, for getting me interested in the topic of solid state quantum devices and for his excellent guidance throughout the entire project. During the past 9 months, I have also benefited greatly from my discussions with Benjamin Joecker; he has played a crucial role in shaping this project. I would also like to thank Andrea Maiani for is very helpful input at times when I got stuck. Lastly, I would also like to thank Albert H. Werner and Daniel Stilck França for their invaluable mentorship during the last three years of my studies and for collaborating with me on research at QMath.

Contents

1 Introduction and Motivation

Quantum computers is a category of devices which utilize quantum mechanical phenomena to perform complex computations. Algorithms such as Grover Search [1], Shor's algorithm [2], and the HHL algorithm [3] have been shown to perform certain computational tasks exponentially faster than known classical algorithms. Quantum computing also has the potential to speed up machine learning algorithms in both the training phase, where the model is built using training data, as wells as the inference phase, where the trained model is used on new data [4]. If this potential is realized, it will greatly benefit the already rapidly expanding usage of machine learning in both scientific and commercial applications. However, these fast quantum algorithms need to run on large fault-tolerant quantum computers and we still lack the knowledge of how to build such devices. Current quantum computers are classified as noisy intermediate-scale quantum (NISQ) devices and they vary considerably in their physical implementation. Trapped ions, superconductors, optical lattices, Bose-Einstein Condensates, and quantum dots are just a few examples of the many different platforms for building quantum computers that are actively being researched [5]. Two obstacles which these platforms have yet to overcome are noise and scalability. Noise collectively refers to unwanted processes in the device which alter its state in an unpredictable fashion and potentially changes the outcome of the computation. Scalability describes how easily the computational capability of the device can be increased.

Spin qubits are a certain type of quantum computing platform where the logical qubit is encoded in the spin degree of freedom of some localized state in a solid-state device. The group-IV semiconductors Si and Ge lend themselves particularly well for implementation of spin-qubits as common isotopes of these have no nuclear spin and can be fabricated to an incredible high purity, making spin qubits in these materials capable of reaching very long coherence times and high fidelity [6]. For the case of Germanium, hole spin-qubits seem especially promising since the hole mobility within Germanium is the highest of all known semiconductors and the strong spin-orbit coupling of the holes allows for fast electrical addressing of the spin as a method for implementing one-qubit gates [7]. Two-qubit operations in such spin-qubit devices often rely on exchange correlations between qubits which are local, so the use of superconductivity to facilitate long-range interaction of qubits is being studied [6, 8]. If it is possible to implement such long-range interactions in a planar device, this type of quantum devices could pave the way for a scalable, noise-robust, and easily addressable platform that can be manufactured using existing methods from the Silicon chip industry.

Motivated by the potential of spin-qubits in Germanium heterostructures as a scalable, noise-robust platform for building quantum computers, the goal of this project is

to develop a method for detailed modeling of such devices. This method shall assist the design of devices that are robust towards noise and allow for accurate two-qubit interactions. The strong spin-orbit coupling in Germanium suggests that the method must be capable of describing the spatial part of the problem in considerable detail. On the basis of this, we start from symmetry-considerations and build an envelope-function model which is then extended to include superconductivity using the Bogoliubov-de Gennes technique. The resulting set of coupled linear partial differential equations are then cast to a weak formulation for numerical solving using a finite-element approach to efficiently obtain eigenstates and eigenvectors close to the Fermi surface. Using the g-matrix formalism, it is demonstrated how the method can be used to determine 'sweet-spots' where the qubits will be robust towards noise in the confinement potential. Lastly, we show how to apply the method to determine coupling coefficients describing the coupling of two quantum dots via a superconductor and study how to tune a physically implemented minimal Kitaev chain to host poor man's Majorana states.

2 $k{\cdot}p$ and Envelope Function Models

Our first task is to determine which physical model we want to use to describe our system. Here we will use the semi-empirical approach of modeling band structures known as the $\boldsymbol{k}\cdot\boldsymbol{p}$ method [9] and subsequently use the envelope function approximation to describe the behaviour of the electrons in the presence of external fields [10].

Our physical system consists of a crystal of Germanium atoms and external magnetic and electric fields. The regular structure of the Germanium crystal means that the system possesses some symmetry if there are no external fields. This invites us to ignore these added fields to begin with so that we can make use of this symmetry and then add the symmetry-breaking fields once we have a model for the pure Germanium crystal. We are interested in studying the behaviour of electrons in Germanium, so we seek a model for the electronic band structure of the material. Our first assumption is that the interaction between electrons can be ignored and that the Germanium nuclei are stationary, so that we can treat it as a one-particle problem. The Hamiltonian describing a single electron moving in a periodic potential V_0 is,

$$H = \frac{p^2}{2m_0^2} + V_0\left(\boldsymbol{r}\right) + \frac{\hbar^2}{4m_0c^2}\boldsymbol{p}\cdot\boldsymbol{\sigma}\times\left(\nabla V_0\right). \tag{1}$$

Here, m_0 is the mass of the free electron, c is the speed of light and $\boldsymbol{\sigma}$ is a vector of Pauli spin matrices. The last term in this expression is the spin-orbit coupling term which originates from the Dirac equation when expanded in the classical limit. The potential $V_0\left(\boldsymbol{r}\right)$ is unchanged under discrete Translation of the coordinate system which is represented as the map $T_{\boldsymbol{R}}$ mapping wave-functions $\Psi\left(\boldsymbol{r}\right)$ to $\Psi\left(\boldsymbol{r}+\boldsymbol{R}\right)$, where $\boldsymbol{R}$ is an element of some discrete set of vectors $\{\boldsymbol{R}\}\subset\mathbb{R}^3$ defining the lattice of the system. From this it follows that H is unchanged under the action of $T_{\boldsymbol{R}}$ for any $\boldsymbol{R}$, which means that we can express eigenstates of H in terms of eigenstates of $T_{\boldsymbol{R}}$. This is the essence of Bloch's theorem. The eigenstates of T_R are of the form $\Psi_{n\boldsymbol{k}}\left(\boldsymbol{r}\right) = e^{i\boldsymbol{k}\cdot\boldsymbol{r}}\left|n\boldsymbol{k}\right\rangle$ where $k_i\in(-\pi/a,\pi/a))$ labels the irreps of T_R, and the $\left|n\boldsymbol{k}\right\rangle$ are periodic i.e. $\left\langle\boldsymbol{r}+\boldsymbol{R}\mid n\boldsymbol{k}\right\rangle = \left\langle\boldsymbol{r}\mid n\boldsymbol{k}\right\rangle$. The quantum number n indexes both the spin of the electron and orbital motion as the SO interaction makes spin not a conserved quantity. In terms of this basis, the Schrödinger equation becomes

$$\left[\frac{p^2}{2m_0} + V_0 + \frac{\hbar^2k^2}{2m_0} + \frac{\hbar}{m_0}\boldsymbol{k}\cdot\boldsymbol{\pi} + \frac{\hbar}{4m_0^2c^2}\boldsymbol{p}\cdot\boldsymbol{\sigma}\times\left(\nabla V_0\right)\right]\left|n\boldsymbol{k}\right\rangle = E_n\left(\boldsymbol{k}\right)\left|n\boldsymbol{k}\right\rangle, \tag{2}$$

were $\boldsymbol{\pi} = \boldsymbol{p} + \frac{\hbar}{4m_0c^2}\sigma\times\nabla V_0$ and we have divided out a factor $e^{i\boldsymbol{k}\cdot\boldsymbol{r}}$ from both sides. In the classical limit ($c\to\infty$) spin becomes a good quantum number and we can write the states $\left|n\boldsymbol{k}\right\rangle\to\left|\nu\boldsymbol{k}\right\rangle\otimes\left|\sigma\right\rangle$ where $u_{\nu\boldsymbol{k}} = \left\langle\boldsymbol{r}|\nu\boldsymbol{k}\right\rangle$ are the *Bloch functions*. Note that Bloch's

theorem for the case $\boldsymbol{k} = 0$ implies that the $u_{\nu 0}$ form a complete orthonormal set of *all* functions with the same periodicity as the lattice, and therefore we can express all Bloch functions $u_{\nu\boldsymbol{k}}(\boldsymbol{r})$ for any $\boldsymbol{k}$ in terms of $u_{\nu 0}$: $u_{\nu k}(\boldsymbol{r}) = \sum_{\nu'} c_{\nu'\nu}(\boldsymbol{k})\, u_{\nu' 0}$.[1] Using this, we define the following basis:

$$|n\boldsymbol{k}\rangle = \sum_{\sigma'\nu'} c_{n\sigma'\nu'}(\boldsymbol{k})\, |\nu'\sigma'\rangle\,, \tag{3}$$

where $|\nu'\sigma'\rangle = |\nu'\boldsymbol{0}\rangle \otimes |\sigma'\rangle$. Plugging this into eq. (2) and multiplying both sides by $\langle\nu\sigma|$ we obtain the $\boldsymbol{k}\cdot\boldsymbol{p}$ Hamiltonian:

$$\sum_{\nu'\sigma'} \left\{ \left[E_{\nu'}(0) + \frac{\hbar^2 k^2}{2m_0} \right] \delta_{\sigma\sigma'}\delta_{\nu\nu'} + \frac{\hbar}{m_0}\boldsymbol{k}\cdot\boldsymbol{P}_{\substack{\nu\nu' \\ \sigma\sigma'}} + \Delta_{\substack{\nu\nu' \\ \sigma\sigma'}} \right\} c_{n\nu'\sigma'}(\boldsymbol{k}) = E_n(\boldsymbol{k}) c_{n\nu\sigma}(\boldsymbol{k}), \tag{4}$$

where

$$\boldsymbol{P}_{\substack{\nu\nu' \\ \sigma\sigma'}} = \left\langle \nu'\sigma' \middle| \left[\boldsymbol{p} + \frac{\hbar}{4m_0c^2}\boldsymbol{\sigma}\times(\nabla V_0) \right] \middle| \nu\sigma \right\rangle, \tag{5a}$$

$$\Delta_{\substack{\nu\nu' \\ \sigma\sigma'}} = \frac{\hbar}{4m_0^2c^2} \langle \nu'\sigma' \mid [\boldsymbol{p}\cdot\boldsymbol{\sigma}\times(\nabla V_0)] \mid \nu\sigma \rangle\,, \tag{5b}$$

and $E_{\nu'}$ is the dispersion relation of the band indexed by ν' with respect to the Hamiltonian in the classical limit. Our choice of basis is independent of the SO interaction, which allows us to treat the SO contributions to $\boldsymbol{P}_{\substack{\nu\nu' \\ \sigma\sigma'}}$ and $\Delta_{\substack{\nu\nu' \\ \sigma\sigma'}}$ perturbatively. When we apply this method to the specific case of Germanium, the band-edge of the top-most valence bands are at the Γ-point which is the reason why we picked the basis in eq. (3) to be expanded around $\boldsymbol{k} = 0$ as the relevant states will be close to this point in the Brillouin zone and we can expand in orders of $\boldsymbol{k}$.

2.1 Envelope Function Approximation

The derivation of the $\boldsymbol{k}\cdot\boldsymbol{p}$ Hamiltonian was based on the translational invariance of the system but a model describing a spin-qubit as a quantum dot in a Germanium heterostructure will have confinement potentials that break discrete translational invariance. The envelope function approximation (EFA) is based on the $\boldsymbol{k}\cdot\boldsymbol{p}$ Hamiltonian and allows for the inclusion of terms in the Hamiltonian that do not possess discrete translational invariance. The source of these terms can be either internal to the material, like e.g. defects, or external, like electrostatic gates or magnetic fields. The central requirement for the applicability of the envelope function approximation is that there is a separation of length scales, in that the additional fields vary appreciably only over length scales much larger than the lattice constant.

[1] In fact, it is possible to show that for any fixed $\boldsymbol{k}$, the set $\{u_{\nu\boldsymbol{k}}\}_\nu$ forms an orthonormal basis of the set of periodic functions [11])

Let us consider the Hamiltonian describing an electron in a lattice in the presence of an electromagnetic field by adding a minimal coupling to eq. (1) as well as a Zeemann term:

$$H = \frac{(-i\hbar\nabla + e\boldsymbol{A})^2}{2m_0} + V + \frac{\hbar}{4m_0^2c^2}\left(-i\hbar\nabla + e\boldsymbol{A}\right)\cdot\boldsymbol{\sigma}\times(\nabla V) + \frac{g_0}{2}\mu\boldsymbol{\sigma}\cdot\boldsymbol{B}. \tag{6}$$

Here, g_0 and e are the g-factor and electric charge of the free electron and $\mu_B = e\hbar/(2m_0)$ is the Bohr magneton. We decompose the electrostatic potential $V = V_0 + V_1$ into the crystal potential V_0 and the slowly varying additional potential V_1. The gradient of the potential is dominated by the crystal potential so we write $\nabla V \approx \nabla V_0$. We also assume that the vector potential, $\boldsymbol{A}$, and the magnetic field, $B = \nabla\times\boldsymbol{A}$, are slowly varying.

Just as in the $\boldsymbol{k}\cdot\boldsymbol{p}$ model, we express the Schrödinger Equation in terms of Bloch functions $u_{\nu'0}(r)\left|\sigma'\right\rangle$, but instead of the plane-wave phase modulation of these Bloch functions we have a more general *envelope function*:

$$\Psi(\boldsymbol{r}) = \sum_{\nu',\sigma'}\psi_{\nu'\sigma'}(\boldsymbol{r})\,u_{\nu'\boldsymbol{0}}(\boldsymbol{r})\left|\sigma'\right\rangle. \tag{7}$$

In this basis, the Schrödinger equation reads:

$$\begin{aligned}\sum_{\nu'\sigma'}\Bigg[&\frac{(-i\hbar\nabla + e\boldsymbol{A})^2}{2m_0} + V_0(\boldsymbol{r}) + \frac{\hbar}{4m_0^2c^2}(-i\hbar\nabla + e\boldsymbol{A})\cdot\boldsymbol{\sigma}\times(\nabla V_0) + V_1(\boldsymbol{r})\\ &+ \frac{g_0}{2}\mu_B\boldsymbol{\sigma}\cdot\boldsymbol{B}\Bigg]\psi_{\nu'\sigma'}(\boldsymbol{r})\,u_{\nu'\boldsymbol{0}}(\boldsymbol{r})\left|\sigma'\right\rangle = E\sum_{\nu'\sigma'}\psi_{\nu'\sigma'}(\boldsymbol{r})\,u_{\nu'\boldsymbol{0}}(\boldsymbol{r})\left|\sigma'\right\rangle.\end{aligned} \tag{8}$$

Periodicity and orthonormality of the Bloch functions imply that

$$\int_{\text{unit cell}}\mathrm{d}\boldsymbol{r}\;u^*_{\nu\boldsymbol{0}}(r)\,u_{\nu'\boldsymbol{0}}(\boldsymbol{r}) = \delta_{\nu\nu'}. \tag{9}$$

Upon multiplying both sides of Equation (8) with $\langle\sigma|\,u^*_{\nu\boldsymbol{0}}(\boldsymbol{r})$ and integrating over a single unit cell, we treat $\boldsymbol{A}(\boldsymbol{r}), \boldsymbol{B}(\boldsymbol{r})$ and $V_1(\boldsymbol{r})$ as constants within the integral so that we obtain the following system of partial differential equations in the envelope-functions $\psi_{\nu'\sigma'}(\boldsymbol{r})$:

$$\begin{aligned}\sum_{\nu'\sigma'}\Bigg\{&\left[E_{\nu'}(\boldsymbol{0}) + \frac{(-i\hbar\nabla + e\boldsymbol{A})^2}{2m_0} + V(\boldsymbol{r})\right]\delta_{\nu\nu'}\delta_{\sigma\sigma'}\\ &+ \frac{1}{m_0}(-i\hbar\nabla + e\boldsymbol{A})\cdot\underset{\sigma\sigma'}{\boldsymbol{P}_{\nu\nu'}} + \underset{\sigma\sigma'}{\Delta_{\nu\nu'}} + \frac{g_0}{2}\mu_B\boldsymbol{\sigma}\cdot\boldsymbol{B}\delta_{\nu\nu'}\Bigg\}\psi_{\nu'\sigma'}(\boldsymbol{r}) = E\psi_{\nu\sigma}(\boldsymbol{r}).\end{aligned} \tag{10}$$

Here $\underset{\sigma\sigma'}{\boldsymbol{P}_{\nu\nu'}}$ and $\underset{\sigma\sigma'}{\Delta_{\nu\nu'}}$ are given by Equations (5a) and (5b) and $E_{\nu'}(\boldsymbol{0})$ is the energy of the Bloch functions with respect to the Hamiltonian in the absence of external fields or

spin-orbit coupling. This infinitely large system of coupled PDEs describes the motion of electrons in our quantum devices, and our next task will be solve this system in order to gain insight into the behavior of our system. In order to make this problem numerically solvable, we first must choose an appropriate finite set of bands ν that are most relevant for the system we are interested in. This is discussed in Section 4.1. Afterwards we can solve the system numerically using the finite element method which we will discuss in Section 5.

2.2 Quasi-2D Systems and the Subband $k \cdot p$ Method

Semiconductor heterostructures are devices where materials with different properties are combined in a non-homogeneous fashion. Such physical systems exhibit interfaces, where the environment changes rapidly as one crosses from one material to another, as well as strain in the materials caused by potentially mismatching lattice structures of the two materials. As the interface contributions are not varying over length scales far longer than the lattice constants of the materials, we would not expect the envelope function approximation to accurately describe such systems. However, it turns out that it is possible to describe electron and hole states in quantum well using the envelope function approximation in good agreement with experiment [12]. In fact, the EFA can be generalized to also apply in situations where the external fields are not slowly varying [13]. A common approach to modeling an interface between two materials in the EFA context is to have the bulk band parameters in the Hamiltonian vary discontinuously at the interface.

The heterostructures we will be looking closer at have a layered structure consisting of a thin layer ($\sim$ 25nm) of Ge sandwiched in between layers of SiGe. If we denote the direction normal to the surface defining the layers (usually called the growth direction) as z, the usual size of the system in the xy-plane is of the order of 10^2nm to 10^3nm. This suggests that the z-direction will not be as important for describing most phenomena within our system. Instead of treating the z-direction in a Finite-element picture, we instead choose to do an approximate diagonalization of the Hamiltonian in what is known as the *subband* $\boldsymbol{k} \cdot \boldsymbol{p}$ *method* [10] to save on computational complexity. As in the regular $\boldsymbol{k} \cdot \boldsymbol{p}$ theory and EFA, the underlying trick in the subband $\boldsymbol{k} \cdot \boldsymbol{p}$ method is to pick a clever basis $\{|m\rangle\}_{m=1}^{\infty}$, to express the Hamiltonian H in, such that the relevant physics is accurately described by a subspace spanned by a finite subset basis vectors $\{|m\rangle\}_{m=1}^{N}$. A common approach to coming up with a clever basis is to take $|m\rangle$ to be eigenstates of some part H_0 of H. Motivated by a desire to describe the growth direction in an analytical fashion we proceed as follows: Let $\{|\eta\rangle\}$ be the solutions to Equation (4) for the case for bulk Germanium (i.e. no interfaces). Expressing Equation (4) in this basis, we can combine all the terms on the left independent of $\boldsymbol{k}$ into $E_\eta(\mathbf{0})$, and the terms proportional to k^2 are combined into $\hbar^2 k^2/(2m_\eta^*)$ where m_η^* is the *effective mass* of the

bulk band η. Usually, $E_\eta(\mathbf{0})$ and m_η^* are obtained approximately either via a Schrieffer-Wolff transformation [10], or simply by treating the $\boldsymbol{k}\cdot\boldsymbol{P}_{\substack{\nu\nu'\\\sigma\sigma'}}$ and $\Delta_{\substack{\nu\nu'\\\sigma\sigma'}}$ as perturbations. Based on this, we define our Hamiltonian H_0 as:

$$(H)_{\eta\eta'} = \delta_{\eta\eta'}\left[-\frac{\hbar^2\,\partial_z^2}{2m_\eta^*} + V(z) + E_\eta(\mathbf{0})\right], \tag{11}$$

where $V(z)$ is a potential that models the confinement in the growth direction due to the change in material. The parameters m_η^* and $E_\eta(\mathbf{0})$ are material specific so in theory they should have a z-dependence and vary discontinuously when passing through the interface between materials. It is possible to include these discontinuous changes in the band parameters but then H_0 will no longer be hermitian. Even though hermiticity can be restored by imposing matching conditions of envelope functions and their derivatives at the boundary, a hermitian formulation of the problem would still neglect microscopic effects of the interface itself, since the band parameters m_η^* and $E_\eta(\mathbf{0})$ are determined based on the bulk models of the materials. We therefore avoid this complication altogether and stick to using Equation (11), while noting that this simplification neglects weak couplings between the in-plane and perpendicular motion. The eigenstates of H_0 we denote as $|\eta m\rangle$ where m denotes the *subband* index. The confinement potential $V(z)$ are sometimes chosen to be either parabolic or that of an infinitely deep quantum well, in which case H_0 becomes analytically solvable. In this work we chose the latter option, in which case the quantum number m takes on integer values, $m \in \mathbb{N}\setminus\{0\}$, and the basis becomes:

$$\langle \boldsymbol{r} \mid \eta\alpha\rangle = \sqrt{\frac{2}{L_z}}\sin\left(m\pi\left[\frac{z}{L_z}+\frac{1}{2}\right]\right)\langle \boldsymbol{r}\mid\eta\rangle, \tag{12}$$

where L_z is the width of the well. Using this basis to express our problem, we argue that, since $\langle \eta m \mid H_0 \mid \eta m\rangle = \mathcal{O}(m^2 L_z^{-2})$, we can use a Schrieffer-Wolff transformation to reduce the problem to only the lowest values of m. Note that for an infinitely deep well, the shape of the bound states only depends on L_z, which means that the subband index m decouples from the bulk band index η and $|\eta m\rangle = |\eta\rangle \otimes |m\rangle$. This allows us to express the problem in a basis that is not necessarily the eigenbasis $|\eta\rangle$ of Equation (4) but instead apply the EFA in the in-plane direction.

3 Bogoliubov-de Gennes Theory

The envelope function approximation in Section 2 describes the behavior of regular particles and holes, but does not involve superconductivity. As one of our goals is to model the superconductive coupling between two spin-qubits, we must extend our model to include superconductivity. The methodology used to achieve this is known as the Bogoliubov-de Gennes method [14] and the main idea is to extend the set of basis functions to also include time-reversed states. The derivation presented here follows that of de Gennes [15], albeit slightly more general.

In second quantization, we will denote the envelope-function Hamiltonian in Equation (10) without superconductivity as

$$\hat{H} = \int\int \mathrm{d}\boldsymbol{r}\mathrm{d}\boldsymbol{r}'\psi_\mu^\dagger(\boldsymbol{r})H_{\mu\nu}\left(\boldsymbol{r},\boldsymbol{r}'\right)\psi_\nu\left(\boldsymbol{r}'\right), \tag{13}$$

where ψ_μ are fermionic field operators which obey the canonical anti-commutation relations,

$$\{\psi_\mu\left(\boldsymbol{r}\right),\psi_\nu\left(\boldsymbol{r}'\right)\} = 0 = \{\psi_\mu^\dagger\left(\boldsymbol{r}\right),\psi_\nu^\dagger\left(\boldsymbol{r}'\right)\},\quad \{\psi_\mu^\dagger\left(\boldsymbol{r}\right),\psi_\nu\left(\boldsymbol{r}'\right)\} = \delta_{\mu\nu}\delta\left(\boldsymbol{r}-\boldsymbol{r}'\right). \tag{14}$$

The indices μ and ν denote the Bloch functions and spin, and when two identical indices appear in the same term we implicitly sum over them. The matrix $H_{\mu\nu}(\boldsymbol{r},\boldsymbol{r}')$ has functions as its elements and can in general contain non-local interactions, which is why it depends on both $\boldsymbol{r}$ and $\boldsymbol{r}'$. To the non-interacting Hamiltonian we now add a two-particle interaction, so that the total Hamiltonian becomes:

$$\mathscr{H} = \int \mathrm{d}\boldsymbol{r}\mathrm{d}\boldsymbol{r}'\left\{\psi_\mu^\dagger(\boldsymbol{r})H_{\mu\nu}\left(\boldsymbol{r},\boldsymbol{r}'\right)\psi_\nu\left(\boldsymbol{r}'\right)+\frac{1}{2}V_{\mu\nu\rho\sigma}\left(\boldsymbol{r}-\boldsymbol{r}'\right)\psi_\mu^\dagger\left(\boldsymbol{r}\right)\psi_\nu^\dagger\left(\boldsymbol{r}'\right)\psi_\rho\left(\boldsymbol{r}'\right)\psi_\sigma\left(\boldsymbol{r}\right)\right\}. \tag{15}$$

In the superconducting state, the electrons of opposite spin can combine into quasi-particles known as Cooper pairs, which means that the operator $\psi_\mu\left(\boldsymbol{r}\right)\psi_\nu\left(\boldsymbol{r}'\right)$ obtains a non-vanishing expectation value. We assume that the coupling V between electrons is weak enough, and that the temperature is not close to the critical temperature, such that we can neglect fluctuations in the density of the quasi-particles and perform the mean-field approximation,

$$\begin{aligned}\psi_\mu^\dagger\left(\boldsymbol{r}\right)\psi_\nu^\dagger\left(\boldsymbol{r}'\right)\psi_\rho\left(\boldsymbol{r}\right)\psi_\sigma\left(\boldsymbol{r}'\right) \rightarrow\ & \left\langle\psi_\mu^\dagger\left(\boldsymbol{r}\right)\psi_\nu^\dagger\left(\boldsymbol{r}'\right)\right\rangle\left\langle\psi_\rho\left(\boldsymbol{r}\right)\psi_\sigma\left(\boldsymbol{r}'\right)\right\rangle \\ &+\psi_\mu^\dagger\left(\boldsymbol{r}\right)\psi_\nu^\dagger\left(\boldsymbol{r}'\right)\left\langle\psi_\rho\left(\boldsymbol{r}\right)\psi_\sigma\left(\boldsymbol{r}'\right)\right\rangle \\ &+\left\langle\psi_\mu^\dagger\left(\boldsymbol{r}\right)\psi_\nu^\dagger\left(\boldsymbol{r}'\right)\right\rangle\psi_\rho\left(\boldsymbol{r}\right)\psi_\sigma\left(\boldsymbol{r}'\right) \\ &+\text{higher order terms}.\end{aligned} \tag{16}$$

If we define the matrix $\Delta(\boldsymbol{r}, \boldsymbol{r}')$ with elements,

$$\Delta_{\mu\nu}(\boldsymbol{r}, \boldsymbol{r}') = V_{\mu\nu\rho\sigma}(\boldsymbol{r} - \boldsymbol{r}') \langle \psi_\rho(\boldsymbol{r}) \psi_\sigma(\boldsymbol{r}') \rangle, \tag{17}$$

the mean-field effective Hamiltonian becomes,

$$\mathscr{H} = \int \mathrm{d}\boldsymbol{r}\mathrm{d}\boldsymbol{r}' \left\{ \psi_\mu^\dagger(\boldsymbol{r}) H_{\mu\nu}(\boldsymbol{r}, \boldsymbol{r}') \psi_\nu(\boldsymbol{r}) + \frac{1}{2} \left[\Delta_{\mu\nu}(\boldsymbol{r}, \boldsymbol{r}') \psi_\mu^\dagger(\boldsymbol{r}) \psi_\nu^\dagger(\boldsymbol{r}') + \text{H.c.} \right] \right\} + \text{const.} \tag{18}$$

This Hamiltonian can be diagonalized using a Bogoliubov transformation, which transforms the fermionic field operators $\psi_\mu^\dagger, \psi_\mu$ representing electrons into another set of fermionic field operators $\gamma_n^\dagger, \gamma_n$ representing quasi-particles. We denote the Bogoliubov transformation as:

$$\psi_\mu(\boldsymbol{r}) = \sum_n u_{n\mu}(\boldsymbol{r}) \gamma_n + v_{n\mu}(\boldsymbol{r}) \gamma_n^\dagger. \tag{19}$$

The functions $u_{n\mu}, v_{n\mu}$ must be chosen such that the quasi-particle fields obey the canonical anti-commutation relations and diagonalize $\mathscr{H}$:

$$\mathscr{H} = E_0 + \sum_n E_n \gamma_n^\dagger \gamma_n. \tag{20}$$

Using the canonical anti-commutation relations, hermiticity of H ($H_{\mu\nu}(\boldsymbol{r}, \boldsymbol{r}') = H_{\nu\mu}^*(\boldsymbol{r}', \boldsymbol{r})$), and $\Delta_{\mu\nu}(\boldsymbol{r}, \boldsymbol{r}') = -\Delta_{\nu\mu}(\boldsymbol{r}', \boldsymbol{r})$, which comes from anti-commutativity of the electronic field operators, we can compute the following commutation relations:

$$[\psi_\lambda(\boldsymbol{r}), \mathscr{H}] = \int \mathrm{d}\boldsymbol{r}' \left\{ H_{\lambda\mu}(\boldsymbol{r}, \boldsymbol{r}') \psi_\mu(\boldsymbol{r}') + \Delta_{\lambda\mu}(\boldsymbol{r}, \boldsymbol{r}') \psi_\mu^\dagger(\boldsymbol{r}') \right\}, \tag{21}$$

$$\left[\psi_\lambda^\dagger(\boldsymbol{r}), \mathscr{H}\right] = \int \mathrm{d}\boldsymbol{r}' \left\{ -H_{\lambda\mu}^*(\boldsymbol{r}, \boldsymbol{r}') \psi_\mu^\dagger(\boldsymbol{r}') + \Delta_{\lambda\mu}^\dagger(\boldsymbol{r}, \boldsymbol{r}') \psi_\mu(\boldsymbol{r}') \right\}, \tag{22}$$

and similarly for the quasi-particle fields:

$$[\gamma_n, \mathscr{H}] = E_n \gamma_n, \tag{23}$$

$$\left[\gamma_n^\dagger, \mathscr{H}\right] = -E_n \gamma_n^\dagger. \tag{24}$$

Expressing the fermionic fields in Equation (21) in terms of the quasi-particle fields and using Equation (23), we get two new equations in terms of $\gamma_n^\dagger, \gamma_n$ and comparing the coefficients in front of these, we find that:

$$E_n u_{n\lambda}(\boldsymbol{r}) = \int \mathrm{d}\boldsymbol{r}' \left\{ H_{\lambda\mu}(\boldsymbol{r}, \boldsymbol{r}') u_{n\mu}(\boldsymbol{r}') + \Delta_{\lambda\mu}(\boldsymbol{r}, \boldsymbol{r}') v_{n\mu}(\boldsymbol{r}) \right\}, \tag{25}$$

$$E_n v_{n\lambda}(\boldsymbol{r}) = \int \mathrm{d}\boldsymbol{r}' \left\{ -H_{\lambda\mu}^*(\boldsymbol{r}, \boldsymbol{r}') v_{n\mu}(\boldsymbol{r}') + \Delta_{\lambda\mu}^\dagger(\boldsymbol{r}, \boldsymbol{r}') u_{n\mu}(\boldsymbol{r}) \right\}. \tag{26}$$

Defining the vector $\boldsymbol{u}_n(\boldsymbol{r})$ with components $u_{n\mu}(\boldsymbol{r})$ (and similarly for $\boldsymbol{v}_n(\boldsymbol{r})$), these equations can be written as a matrix equation:

$$\int \mathrm{d}\boldsymbol{r'} \begin{pmatrix} H(\boldsymbol{r},\boldsymbol{r'}) & \Delta(\boldsymbol{r},\boldsymbol{r'}) \\ \Delta^\dagger(\boldsymbol{r},\boldsymbol{r'}) & -H^*(\boldsymbol{r},\boldsymbol{r'}) \end{pmatrix} \begin{pmatrix} \boldsymbol{u}_n(\boldsymbol{r'}) \\ \boldsymbol{v}_n(\boldsymbol{r'}) \end{pmatrix} = E_n \begin{pmatrix} \boldsymbol{u}_n(\boldsymbol{r}) \\ \boldsymbol{v}_n(\boldsymbol{r}) \end{pmatrix}. \tag{27}$$

These are the Bogoliubov-de Gennes equations, and in the absence of the two-particle interaction ($V\mu\nu\rho\sigma = 0$) this system of PDEs decouples into the regular Schrödinger equation and its time-reversed counterpart:

$$\int \mathrm{d}\boldsymbol{r'} H(\boldsymbol{r},\boldsymbol{r'})\boldsymbol{u}_n(\boldsymbol{r'}) = E_n \boldsymbol{u}_n(\boldsymbol{r'}), \tag{28}$$

$$\int \mathrm{d}\boldsymbol{r'} H(\boldsymbol{r},\boldsymbol{r'})\boldsymbol{v}_n^*(\boldsymbol{r'}) = -E_n \boldsymbol{v}_n^*(\boldsymbol{r'}). \tag{29}$$

The time-reversal operator is an anti-unitary operator and can be expressed as the combination $\Theta = U\mathcal{K}$ where U is a unitary operator and $\mathcal{K}$ is the complex conjugation operator acting on functions as: $\mathcal{K}f(\boldsymbol{r}) = f^*(\boldsymbol{r})$. It is common to transform the Bogolibov-de Gennes equations using the unitary transformation $\mathbb{1} \oplus U$, so that it becomes

$$\int \mathrm{d}\boldsymbol{r'} \begin{pmatrix} H(\boldsymbol{r},\boldsymbol{r'}) & \Delta(\boldsymbol{r},\boldsymbol{r'})U^\dagger \\ U\Delta^\dagger(\boldsymbol{r},\boldsymbol{r'}) & -\Theta H(\boldsymbol{r},\boldsymbol{r'})\Theta^{-1} \end{pmatrix} \begin{pmatrix} \boldsymbol{u}_n(\boldsymbol{r'}) \\ \boldsymbol{v}_n(\boldsymbol{r'}) \end{pmatrix} = E_n \begin{pmatrix} \boldsymbol{u}_n(\boldsymbol{r}) \\ \boldsymbol{v}_n(\boldsymbol{r}) \end{pmatrix}, \tag{30}$$

where we have used that $H^* = \mathcal{K}H\mathcal{K}$. These equations reproduce the usual BCS description of superconductivity when u_n and v_n are regular two-component spinors and the superconductive coupling $\Delta(\boldsymbol{r},\boldsymbol{r'}) = \Delta(\boldsymbol{r})\delta(\boldsymbol{r}-\boldsymbol{r'})i\sigma_y$ with σ_y being the Pauli y-matrix [16]. The time-reversal operator in this case becomes $i\sigma_y\mathcal{K}$.

3.1 Proximitized Superconductivity

In the BdG Equation (30) superconductivity emerges when the order parameter Δ is present, which in turn implies an attractive interaction between the particles in the material, $V \neq 0$. In regular Germanium, superconductivity does not manifest, but if the material is brought into contact with a superconductor it is possible for an effective Δ to emerge in the Germanium [17, 18]. This effect is known as the *proximity effect*, and a heuristic argument for this effect is that Cooper pairs can "leak" out of the superconductor such that the operator $\psi_\mu(\boldsymbol{r})\psi_\nu(\boldsymbol{r'})$ obtains a non-vanishing expectation value in the Germanium. This intuition can be made more rigorous by considering the combined interacting system of Germanium and superconductor studying how the propagator in the Germanium system is renormalized due to the presence of the superconductor. Studying the Green's function for superconductive systems is elegantly done in the Nambu formalism. Let $\Psi_\mu^\dagger(\boldsymbol{r}), \Psi_\mu(\boldsymbol{r})$ be the field operators describing fermions in the superconductor.

The index μ denotes all relevant internal degrees of freedom such as spin, band index etc. The Hamiltonian in the superconductor is of the form:

$$\mathscr{H}^{\mathrm{SC}} = \int \mathrm{d}\boldsymbol{r}\Psi_\mu^\dagger(\boldsymbol{r})h_{\mu\nu}^{\mathrm{SC}}(\boldsymbol{r})\Psi_\nu(\boldsymbol{r}) + \int \mathrm{d}\boldsymbol{r}\mathrm{d}\boldsymbol{r'}\Delta_{\mu\nu}(\boldsymbol{r},\boldsymbol{r'})\Psi_\mu^\dagger(\boldsymbol{r'})\Psi_\nu^\dagger(\boldsymbol{r'}) + \mathrm{H.c.} \tag{31}$$

Introducing the Nambu spinor $\underline{\Psi} = \begin{pmatrix}\Psi & \Psi^\dagger\end{pmatrix}^T$ where Ψ is a vector with elements Ψ_μ. $\Psi^\dagger$ is also a vector of the same dimension as Ψ, but with time-reversed ordering of the elements which we will label as $\Psi_{\bar{\mu}}^\dagger$. This ordering allows us, in full analogy to the BdG derivation, to write:

$$\mathscr{H}^{\mathrm{SC}} = \int \mathrm{d}\boldsymbol{r}\mathrm{d}\boldsymbol{r'}\underline{\Psi}^\dagger(\boldsymbol{r})H^{\mathrm{SC}}(\boldsymbol{r},\boldsymbol{r'})\underline{\Psi}(\boldsymbol{r'}) + \mathrm{const.} \tag{32}$$

with

$$H^{\mathrm{SC}} = \frac{1}{2}\begin{pmatrix} h^{\mathrm{SC}} & \Delta \\ \Delta^\dagger & -\Theta h^{\mathrm{SC}}\Theta^{-1}\end{pmatrix}, \tag{33}$$

where we have absorbed a unitary matrix into Δ. The Matsubara Green's function in Nambu space is defined as

$$\underline{\underline{\mathcal{G}}}(\boldsymbol{r},\boldsymbol{r'},\tau) = -\left\langle T_\tau \underline{\Psi}(\boldsymbol{r},\tau)\otimes\underline{\Psi}^\dagger(\boldsymbol{r'},0)\right\rangle, \tag{34}$$

where T_τ is the time-ordering operator and $\otimes$ denotes the outer product of the Nambu spinors. If the band index μ runs over N elements, the Nambu Green's function is a $2N\times 2N$ matrix. The Nambu Green's function can also be divided into four $N\times N$ blocks,

$$\underline{\underline{\mathcal{G}}}(\boldsymbol{r},\boldsymbol{r'},\tau) = \begin{pmatrix}\mathcal{G}_{\mathrm{p}}(\boldsymbol{r},\boldsymbol{r'},\tau) & \mathcal{G}_{\mathrm{ph}}^*(\boldsymbol{r},\boldsymbol{r'},\tau)\\ \mathcal{G}_{\mathrm{ph}}(\boldsymbol{r},\boldsymbol{r'},\tau) & \mathcal{G}_{\mathrm{p}}^*(\boldsymbol{r},\boldsymbol{r'},\tau)\end{pmatrix}, \tag{35}$$

with

$$\mathcal{G}_{\mathrm{p}}(\boldsymbol{r},\boldsymbol{r'},\tau) = -\left\langle T_\tau \Psi(\boldsymbol{r},\tau)\otimes\Psi^\dagger(\boldsymbol{r'},0)\right\rangle, \tag{36}$$

$$\mathcal{G}_{\mathrm{ph}}(\boldsymbol{r},\boldsymbol{r'},\tau) = -\left\langle T_\tau \Psi^\dagger(\boldsymbol{r},\tau)\otimes\Psi^\dagger(\boldsymbol{r'},0)\right\rangle. \tag{37}$$

The Hamiltonian describing the dynamics in Germanium can also be expressed in the Nambu formalism. If we denote the creation operator of a particle in Germanium in the state μ at position $\boldsymbol{r}$ by $\psi_\mu^\dagger(\boldsymbol{r})$, we can write

$$\mathscr{H}^{\mathrm{Ge}} = \int \mathrm{d}\boldsymbol{r}\psi_\mu^\dagger(\boldsymbol{r})h_{\mu\nu}^{\mathrm{Ge}}(\boldsymbol{r})\psi_\nu(\boldsymbol{r}) = \int \mathrm{d}\boldsymbol{r}\mathrm{d}\boldsymbol{r'}\underline{\psi}^\dagger(\boldsymbol{r})H^{\mathrm{Ge}}(\boldsymbol{r},\boldsymbol{r'})\underline{\psi}(\boldsymbol{r'}) + \mathrm{const.} \tag{38}$$

with

$$H^{\mathrm{Ge}} = \frac{1}{2}\begin{pmatrix} h^{\mathrm{Ge}} & 0\\ 0 & -\Theta h^{\mathrm{Ge}}\Theta^{-1}\end{pmatrix}. \tag{39}$$

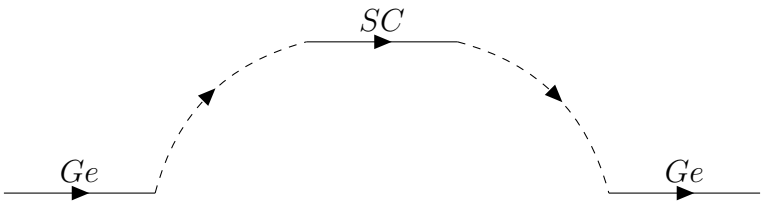

Figure 1: Irreducible Feynman diagram for the Germanium Green's function. The solid lines labeled "Ge" and "SC" represent the free Green's function in Germanium and the superconductor respectively and the dashed lines indicate the tunneling process t.

For this system we can also define a Matsubara Green's function in Nambu space in exact analogy with Equations (34) and (35). The coupling of the superconductor $\mathscr{H}^{\mathrm{SC}}$ and the Germanium system $\mathscr{H}^{\mathrm{Ge}}$ is described by in a tunneling picture, where a particle tunnels from the Germanium system to the superconductor. The general expression for this tunnel process can be written as:

$$\mathscr{H}^{\mathrm{t}} = \int \mathrm{d}\boldsymbol{r}\mathrm{d}\boldsymbol{r'}\psi^{\dagger}_{\mu}(\boldsymbol{r})t_{\mu\nu}(\boldsymbol{r},\boldsymbol{r'})\Psi_{\nu}(\boldsymbol{r'}) + \mathrm{H.c.} \tag{40}$$

Our goal is to integrate out the degrees of freedom in the superconductor to obtain an effective model of the Germanium system. We therefore want to compute the renormalized propagator in the Germanium system. In the absence of interactions with the superconductor, the particle number in the Germanium is conserved and the anomalous Green's function, $\mathcal{G}^{(\mathrm{Ge})}_{ph}$, vanishes. In the presence of interactions, however, a particle in the Germanium can tunnel into the superconductor, combine with another particle and condense into a Cooper pair, leaving an anti-particle, which can then tunnel back out into the Germanium. The Feynman diagram corresponding to this is given in Figure 1, and this process is the only irreducible diagram possible. Hence, the self-energy becomes:

$\underline{\underline{\Sigma}}(\boldsymbol{r},\tau,\boldsymbol{r'},\tau') =$  $= \int \mathrm{d}\boldsymbol{r}_1\mathrm{d}\boldsymbol{r}_2\underline{t}(\boldsymbol{r},\boldsymbol{r_2})\underline{\underline{\mathcal{G}}}^{\mathrm{SC}}(\boldsymbol{r}_2,\boldsymbol{r}_1,\tau-\tau')\underline{t}^{\dagger}(\boldsymbol{r_1},\boldsymbol{r'}),$ (41)

where $\underline{t} = t \oplus \Theta t^{\dagger}\Theta^{-1}$ is the Nambu-space representation of the tunneling process. Including this to all orders in t in the renormalized propagator in Germanium using the Dyson equation, the renormalized propagator in Germanium, becomes:

$$\underline{\underline{\mathcal{G}}}(\boldsymbol{r},\boldsymbol{r'},i\omega) = \frac{1}{(\underline{\underline{\mathcal{G}^{(0)}}})^{-1}(\boldsymbol{r},\boldsymbol{r'},i\omega) - \underline{\underline{\Sigma}}(\boldsymbol{r},\boldsymbol{r'},i\omega)} = \frac{1}{i\omega - H^{\mathrm{Ge}}(\boldsymbol{r})\delta(\boldsymbol{r}-\boldsymbol{r'}) - \underline{\underline{\Sigma}}(\boldsymbol{r},\boldsymbol{r'},i\omega)}. \tag{42}$$

From this we can obtain an effective Hamiltonian if we can treat the self-energy as frequency independent, so that the Hamiltonian

$$H^{\mathrm{Ge}}_{\mathrm{eff}}(\boldsymbol{r},\boldsymbol{r'}) = H^{\mathrm{Ge}}(\boldsymbol{r})\delta(\boldsymbol{r}-\boldsymbol{r'}) + \underline{\underline{\Sigma}}(\boldsymbol{r},\boldsymbol{r'}), \tag{43}$$

reproduces the same dynamics as described by Equation (42), in the sense that the spectrum of $H_{\text{eff}}^{\text{Ge}}$ matches the poles of Equation (42).

Single Band s-wave Superconductor

In order to make the above description of how to obtain an effective Hamiltonian capturing the proximity effect in Germanium more concrete, we consider a simple model for the superconductor, in a generalization of [19] (see also [20]). The superconductor is modeled as a single band in the effective mass approximation. The superconductive coupling pairs electrons of opposite spin and momentum, and we assume that Δ is independent of momentum. In momentum space, we have:

$$\mathscr{H}^{\text{SC}} = \sum_{\boldsymbol{k},\sigma} \Psi^\dagger_{\boldsymbol{k}\sigma}\xi_{\boldsymbol{k}}\Psi_{\boldsymbol{k}\sigma} - \sum_k \left[\Delta\Psi^\dagger_{\boldsymbol{k}\uparrow}\Psi^\dagger_{-\boldsymbol{k}\downarrow} + \Delta^*\Psi_{-\boldsymbol{k}\downarrow}\Psi_{\boldsymbol{k}\uparrow}\right], \tag{44}$$

with $\xi_{\boldsymbol{k}} = \hbar^2 \left\|\boldsymbol{k}\right\|^2/(2m^*_{\text{SC}}) - \mu$ and m^*_{SC} and μ being the effective mass and chemical potential in the superconductor. For the Germanium system we expand in terms of Bloch functions in the limit of vanishing spin-orbit just as in the $k\cdot p$-model in Section 2. We therefore index the field operator in Germanium $\psi_{\mu\sigma}$ by a Bloch function index μ and a spin index σ. We also assume that the system is two-dimensional and fix the z-direction perpendicular to the plane where the Germanium heterostructure is. For the tunneling between the Germanium structure and the superconductor we assume it to be local and spin-preserving:

$$t_{\mu\sigma,\sigma'}(\boldsymbol{r},\boldsymbol{r'}) = \tilde{t}\delta(x-x')\delta(y-y')\delta(z')\delta_{\sigma\sigma'}. \tag{45}$$

In this expression for the tunnel coupling we have also placed the Germanium heterostructure at $z=0$. If we define $\boldsymbol{r}_\parallel = (r_x, r_y, 0)^T$ and assume that the volume of the superconductor $V = L_z A$ with A being the area of the Germanium heterostructure, we can compute the momentum space representation of the interaction term:

$$\begin{aligned}
\mathscr{H}^{\text{t}} &= \tilde{t}\sum_{\mu,\sigma}\int \mathrm{d}\boldsymbol{r}_\parallel \mathrm{d}\boldsymbol{r}' \frac{1}{A\sqrt{L_z}} \sum_{\boldsymbol{k}_\parallel,\boldsymbol{k}'} e^{i\boldsymbol{k}_\parallel\cdot\boldsymbol{r}_\parallel - i\boldsymbol{k}'\cdot\boldsymbol{r}'} c^\dagger_{\boldsymbol{k}_\parallel\mu\sigma} d_{\boldsymbol{k}'\sigma}\delta(x-x')\delta(y-y')\delta(z') + \text{H.c.} \\
&= \frac{\tilde{t}}{A\sqrt{L_z}}\sum_{\mu,\sigma}\int \mathrm{d}x\mathrm{d}y \sum_{\boldsymbol{k}_\parallel,\boldsymbol{k}'} e^{i(\boldsymbol{k}_\parallel-\boldsymbol{k}')\cdot\boldsymbol{r}_\parallel} c^\dagger_{\boldsymbol{k}_\parallel\mu\sigma} d_{\boldsymbol{k}'\sigma} + \text{H.c.} \\
&= t\sum_{\mu,\sigma}\sum_{\boldsymbol{k}}\left[c^\dagger_{\boldsymbol{k}_\parallel\mu\sigma} d_{\boldsymbol{k}\sigma} + d^\dagger_{\boldsymbol{k}\sigma} c_{\boldsymbol{k}_\parallel\mu\sigma}\right]
\end{aligned} \tag{46}$$

Here, $t = \tilde{t}/(A\sqrt{L_z})$, and

$$c_{\boldsymbol{k}_\parallel\mu\sigma} = A^{-\frac{1}{2}}\int \mathrm{d}\boldsymbol{r}_\parallel \psi_{\mu\sigma}(\boldsymbol{r}_\parallel)e^{i\boldsymbol{k}_\parallel\cdot\boldsymbol{r}_\parallel}, \tag{47}$$

$$d_{\boldsymbol{k}\sigma} = V^{-\frac{1}{2}}\int \mathrm{d}\boldsymbol{r}\Psi_\sigma(\boldsymbol{r})e^{i\boldsymbol{k}\cdot\boldsymbol{r}}. \tag{48}$$

When tunneling into the superconductor, the particle "forgets" which Bloch function it was and the spin-index is the only internal degree of freedom. When the particle tunnels back out of the superconductor it can become any Bloch function as well. This means that the effective superconductive order parameter in the Germanium system will couple states to more than just their time-reversed counterparts. Evaluating the self-energy Equation (41) for these descriptions of the superconductor and tunnel coupling we get,

$$\underline{\underline{\Sigma}}_{\mu\nu}(\boldsymbol{k}_\parallel, \tau - \tau') = \sum_{k_z} \begin{pmatrix} \mathcal{G}_{\mathrm{p}}^{\mathrm{SC}}(\boldsymbol{k}, \tau - \tau')|t|^2|\mu\rangle\langle\nu| & \mathcal{G}_{\mathrm{ph}}^{\mathrm{SC}*}(\boldsymbol{k}, \tau - \tau')t^2|\mu\rangle\langle\overline{\nu}| \\ \mathcal{G}_{\mathrm{ph}}^{\mathrm{SC}}(\boldsymbol{k}, \tau - \tau')(t^*)^2|\overline{\mu}\rangle\langle\nu| & \mathcal{G}_{\mathrm{p}}^{\mathrm{SC}*}(\boldsymbol{k}, \tau - \tau')|t|^2|\overline{\mu}\rangle\langle\overline{\nu}| \end{pmatrix}. \tag{49}$$

In order to simplify notation we define the operators T_p and T_{ph}, acting on the Bloch-function subspace, with elements:

$$(T_p)_{\mu\nu} = |t|^2|\mu\rangle\langle\nu|, \qquad (T_{ph})_{\mu\nu} = t^2|\mu\rangle\langle\overline{\nu}|, \tag{50}$$

and combine these into the matrix

$$\underline{\underline{T}} = \begin{pmatrix} T_p & T_{ph} \\ T_{ph}^\dagger & \Theta T_p \Theta^{-1} \end{pmatrix}. \tag{51}$$

With this, the expression for the self-energy simplifies to

$$\underline{\underline{\Sigma}}(\boldsymbol{k}_\parallel, \tau - \tau') = \sum_{k_z} \underline{\underline{\mathcal{G}}}^{\mathrm{SC}}(\boldsymbol{k}, \tau - \tau') \circ \underline{\underline{T}}, \tag{52}$$

where $\circ$ denotes the Hadamard product which multiplies matrices of the same shape element-wise i.e. $A = B \circ C$ has elements $A_{ij} = B_{ij}C_{ij}$. We can express the self-energy in terms of Matsubara frequencies using a Fourier transform of the imaginary time:

$$\begin{aligned} \underline{\underline{\Sigma}}(\boldsymbol{k}_\parallel, i\omega) &= \int_0^\beta \mathrm{d}\tau e^{i\omega\tau} \underline{\underline{\Sigma}}(\boldsymbol{k}_\parallel, i\omega) \ = \int_0^\beta \mathrm{d}\tau e^{i\omega\tau} \sum_{k_z} \underline{\underline{\mathcal{G}}}^{\mathrm{SC}}(\boldsymbol{k}, \tau) \circ \underline{\underline{T}} \\ &= \frac{1}{\beta} \sum_{i\omega'} \int_0^\beta \mathrm{d}\tau e^{i(\omega - \omega')\tau} \sum_{k_z} \underline{\underline{\mathcal{G}}}^{\mathrm{SC}}(\boldsymbol{k}, i\omega') \circ \underline{\underline{T}} \\ &= \frac{1}{\beta} \sum_{i\omega'} \beta\delta(\omega - \omega') \sum_{k_z} \underline{\underline{\mathcal{G}}}^{\mathrm{SC}}(\boldsymbol{k}, i\omega') \circ \underline{\underline{T}} = \sum_{k_z} \underline{\underline{\mathcal{G}}}^{\mathrm{SC}}(\boldsymbol{k}, i\omega) \circ \underline{\underline{T}}. \end{aligned} \tag{53}$$

The sum over z-momenta can be replaced by a sum over energies using the density of states $\nu(\epsilon, \boldsymbol{k}) := \sum_{k_z} \delta(\epsilon - \epsilon_{\boldsymbol{k}})$ where $\epsilon_k = \xi_{\boldsymbol{k}} + \mu$ is the dispersion in the superconductor.

$$\underline{\underline{\Sigma}}(\boldsymbol{k}_\parallel, i\omega) = \int \mathrm{d}\epsilon \ \nu(\epsilon, \boldsymbol{k}_\parallel) \underline{\underline{\mathcal{G}}}^{\mathrm{SC}}(\epsilon, i\omega) \circ \underline{\underline{T}}. \tag{54}$$

The Green's function in the superconductor is [21]:

$$\underline{\underline{\mathcal{G}}}^{\mathrm{SC}}(\epsilon, i\omega) = \frac{1}{\omega^2 + \epsilon^2 + |\Delta_0|^2} \begin{pmatrix} -i\omega - \epsilon & \Delta_0 i\sigma_y \\ -i\Delta_0^* \sigma_y & -i\omega + \epsilon \end{pmatrix}, \tag{55}$$

and σ_y is the Pauli y-matrix acting in the spin-space for the superconductor. If $\Delta_0, \omega \ll \epsilon_F$, only the states close the Fermi surface are relevant, and we can treat the density of states ν as constant. If we assume this to be the case, the integral over the energy in eq. (54) can readily be evaluated, giving

$$\underline{\underline{\Sigma}}(\boldsymbol{k}_\parallel, i\omega) = \frac{\pi\nu}{\sqrt{|\Delta_0|^2+\omega^2}} \begin{pmatrix} -i\omega & \Delta_0 i\sigma_y \\ -i\Delta_0^* \sigma_y & -i\omega \end{pmatrix} \circ \underline{\underline{T}}. \tag{56}$$

With this expression of the self-energy, we can determine the renormalized propagator for the particles in Germanium. Defining $\gamma(i\omega) = \frac{\pi\nu}{\sqrt{|\Delta_0|^2+\omega^2}}$, we have

$$\begin{aligned} \underline{\underline{\mathcal{G}}}^{-1}(\boldsymbol{k}_\parallel, i\omega) &= \underline{\underline{\mathcal{G}^{(0)}}}\left(\boldsymbol{k}_\parallel, i\omega\right) - \underline{\underline{\Sigma}}(\boldsymbol{k}_\parallel, i\omega) \\ &= i\omega - \begin{pmatrix} h^{\mathrm{Ge}}(\boldsymbol{k}_\parallel) & 0 \\ 0 & -\Theta h^{\mathrm{Ge}}(\boldsymbol{k}_\parallel)\Theta^{-1} \end{pmatrix} - \gamma(i\omega) \begin{pmatrix} -i\omega & \Delta_0 i\sigma_y \\ -i\Delta_0^* \sigma_y & -i\omega \end{pmatrix} \circ \underline{\underline{T}} \\ &= i\omega \begin{pmatrix} 1+\gamma(i\omega)T_p & 0 \\ 0 & 1+\gamma(i\omega)\Theta T_p \Theta^{-1} \end{pmatrix} - \begin{pmatrix} h^{\mathrm{Ge}}(\boldsymbol{k}_\parallel) & \gamma(i\omega)\Delta_0 i\sigma_y T_{ph} \\ -\gamma(i\omega)\Delta_0^* i\sigma_y T_{ph}^\dagger & -\Theta h^{\mathrm{Ge}}(\boldsymbol{k}_\parallel)\Theta^{-1} \end{pmatrix}. \end{aligned} \tag{57}$$

In order to obtain an effective Hamiltonian describing the low-energy behaviour, we assume that dynamical effects are negligible for energies below the gap $\omega < \Delta_0$ which allows us to expand the self-energy to first order in ω. Doing so, we find

$$\underline{\underline{\mathcal{G}}}^{-1}(\boldsymbol{k}_\parallel, i\omega) \approx \left[i\omega - H_{eff}^{\mathrm{Ge}}\right](\tau_0 \circ (1 + \gamma \underline{\underline{T}})), \tag{58}$$

where $\gamma = \gamma(0) = \pi\nu/|\Delta_0|$ and the effective Hamiltonian

$$H_{eff}^{\mathrm{Ge}} = \begin{pmatrix} h^{\mathrm{Ge}}(\boldsymbol{k}_\parallel)(1+\gamma T_p)^{-1} & i\sigma_y \Delta_0 T_{ph}(\gamma^{-1} + \Theta T_p \Theta^{-1})^{-1} \\ -i\sigma_y \Delta_0^* T_{ph}^\dagger (\gamma^{-1} + T_p)^{-1} & -\Theta h^{\mathrm{Ge}}(\boldsymbol{k}_\parallel)(1+\gamma T_p)^{-1}\Theta^{-1} \end{pmatrix}. \tag{59}$$

The term $\tau_0 \circ (1 + \gamma \underline{\underline{T}})$ is independent of ω and always invertible since $\underline{\underline{T}}$ is positive semi-definite, so we identify it as the renormalization constant. The poles are entirely determined by $\left[i\omega - H_{eff}^{\mathrm{Ge}}\right]$, meaning that the effective Hamiltonian describes the same dynamics as the renormalized Green's function eq. (58). Inspecting the diagonal blocks in the effective Hamiltonian, we see that the presence of the superconductor introduces new coupling terms between the Bloch functions which become more dominant as $|\Delta_0|$ decreases. The intuition for these terms is that the particles can enter the superconductor as one Bloch function and come back out as another but still remain a particle. For the same reason, the off-diagonal elements couple Bloch functions that are not necessarily time-reversals of each other.

There are multiple ways to generalize this description of the proximity effect. For example, one could make the tunnel coupling be different for the Bloch functions in Germanium by replacing the scalars t and t^* in Equation (50) with matrices that depend

on μ and ν. One could also study different types of superconductors by altering the superconductive Green's function in the self-energy eq. (54) or even add more bands to the superconductor by extending the superconductive Nambu-Green's function from a 4×4 matrix structure to a $4n \times 4n$ matrix as well as extending the $\underline{\underline{T}}$ matrix with a $2n \times 2n$ matrix and tracing out these added bands in the Hadamard product in the self-energy.

With the effective Hamiltonian Equation (59) expressed in the basis of Bloch functions in the limit of vanishing spin-orbit interaction, we can use the envelope-function approximation from Section 2.1 to also describe systems where the tunnel process is spatially dependent. This will be relevant when we look closer at the coupling of quantum dots (which are not connected to a superconductor) and (proximitized) superconductors in Section 7. In this work, we will not use this tunneling approach to determine the effective Hamiltonian describing the proximity effect, but rather argue based on symmetry considerations how the effective superconductive order parameter in the effective Hamiltonian can look. The magnitude of this order parameter we will set to match the measured coupling strength in experimental devices, and we will assume that this magnitude is large enough so that we can ignore the factor $(1 + \gamma T_p)^{-1}$ in the diagonal blocks of the effective Hamiltonian.

4 Theory of Invariants

Bloch's theorem, which we used to derive the $\boldsymbol{k}\cdot\boldsymbol{p}$ Hamiltonian in Section 2 uses only discrete translational invariance of the system, but many crystals will also be invariant under certain improper rotations. This additional symmetry provides a convenient way of determining how the Hamiltonian in Equation (4) can couple different Bloch functions based on symmetry considerations alone without knowing the explicit form of the $u_{\nu\boldsymbol{k}}$. This approach is known as the *theory of invariants*, and we will use this to determine the general form of not only the regular Hamiltonian describing holes in Germanium heterostructures but also the superconductive coupling Δ in the BdG extension. The additional symmetry of the problem can be phrased as the invariance of the crystal potential V_0 under a unitary representation of a given *point group* which is a subgroup of the set of improper rotations (the set of all spatial rotations and inversions: $SU(2)\times C_2$). For the case $\boldsymbol{k}=0$ this means that the Hamiltonian on the left-hand side of Equation (2) commutes with the representation of the point group. In the following, we will derive the theory of invariants in a general context to keep the notation simple. The approach follows that of [22].

Let $\mathcal{G}$ be a group, and denote the representation of $\mathcal{G}$ on real space ($\mathbb{R}^3$) as Gx where $x\in\mathbb{R}^3$. Let $\{\psi_i\}_{i=1}^n$ be an orthogonal family of n wavefunctions defined on $\mathbb{R}^3$ which transforms in the following way under the action of the group:

$$\psi_i(G^{-1}x)=\sum_j D_{ij}(G)\psi_j(x)$$

for any $G\in\mathcal{G}$. This expression implies that D is an n-dimensional unitary representation of $\mathcal{G}$. Let $\mathcal{H}(\mathcal{K})$ be a Hamiltonian described as a matrix which acts on the ψ_is and depends on a tensor $\mathcal{K}$ describing e.g. the electric field, the wave-vector or other operators. Under the action of $\mathcal{G}$, $\mathcal{H}$ will then transform as:

$$\mathcal{H}(\mathcal{K})\to D^{-1}(G)\mathcal{H}(\mathcal{K})D(G). \tag{60}$$

If the system we are modeling is invariant with respect to the action of $\mathcal{G}$, this means that

$$D(G)\mathcal{H}(G^{-1}\mathcal{K})D^{-1}(G)=\mathcal{H}(\mathcal{K}). \tag{61}$$

We can view $\mathcal{H}$ as a vector in the space $\mathbb{C}^{n\times n}$ which has the canonical basis $X^{lk}\in\mathbb{C}^{n\times n}$ given by:

$$(X^{lk})_{l'k'}=\delta_{ll'}\delta_{kk'}. \tag{62}$$

In this new vector space, the representation of $\mathcal{G}$ induced by D transforms the basis vectors X^{lk} in the following way:

$$G^{-1}X^{lk}=D(G)X^{lk}D^{-1}(G) \tag{63}$$

It is straight-forward to show that this transformation is linear and unitary, so we conclude that this is an n^2-dimensional representation of $\mathcal{G}$. We can express this representation as unitary matrices $\mathcal{D}^{(X)} \in \mathbb{C}^{n^2 \times n^2}$ acting on the basis vectors X^{lk}:

$$G^{-1} X^{lk} = \sum_{l'k'} X^{l'k'} D^{(X)}_{ll'kk'}(G) \tag{64}$$

Using Equation (63), we can express the matrix elements of $D^{(X)}$ in terms of the original representation D:

$$(G^{-1} X^{lk})_{l'k'} = \sum_{ij} D_{l'i}(G)(X^{lk})_{ij} D^{-1}_{jk'}(G) = D_{l'l}(G) D^{-1}_{kk'}(G) = D_{l'l}(G) D^{\dagger}_{kk'}(G) \tag{65}$$

where we have used unitarity of D in the last step. From this we see that $D^{(X)}$ is simply the tensor product $D \otimes D^*$ where D^* is the adjoint representation of D given by $\mathcal{G} \ni G \mapsto D^{\dagger}(G)$. A central concept in the field of representation theory is the invariant subspace. An invariant subspace of $D^{(X)}$ is a subspace $V \subset \mathbb{C}^{n \times n}$ which is closed under $D^{(X)}$ i.e. for all $G \in \mathcal{G}$ and any $M \in V$

$$D^{(X)}(G) M \in V. \tag{66}$$

If there a non-trivial invariant subspace $V \neq 0$ or $\mathbb{C}^{n \times n}$ exists, then we say that the representation $D^{(X)}$ is reducible. If no non-trivial invariant subspace exists, $D^{(X)}$ is an irreducible representation (irrep). Even if D may be irreducible, $D^{(X)} = D \otimes D^*$ will in general be reducible. By Schur's lemma [23], this means that we can express $D^{(X)}$ in block diagonal form with respect to some basis consisting of n^2 matrices $\{X^{\lambda}_i\} \subset \mathbb{C}^{n \times n}$. Here, λ labels the invariant subspace that X^{λ}_i belongs to. In this basis, the Hamiltonian $\mathcal{H}$ takes the form:

$$\mathcal{H} = \sum_{\lambda} \sum_{i} \alpha_{\lambda,i}(\mathcal{K}) X^{\lambda}_i. \tag{67}$$

We can apply exactly the same approach to the tensor $\mathcal{K}$, and determine a basis of tensors $\{\mathcal{K}^{\lambda}_i\}$ belonging to the different invariant subspaces. Doing so, we get that the Hamiltonian becomes,

$$\mathcal{H} = \sum_{\lambda} \alpha_{\lambda} \sum_{i} X^{(\lambda)}_l \mathcal{K}^{(\lambda)}_i. \tag{68}$$

If the representation D is reducible, we can express the matrices X^{λ}_i in the basis $\{\psi^{\lambda'}_i\}_{\lambda,i}$ where D is block diagonal $D = \bigoplus_{\lambda'} D_{\lambda'}$. Doing so, the Hamiltonian can be split up into blocks

$$\mathcal{H}(\mathcal{K}) = \begin{pmatrix} \mathcal{H}_{11} & \mathcal{H}_{12} & \dots \\ \mathcal{H}_{21} & \ddots & \\ \vdots & & \end{pmatrix} \tag{69}$$

where $\mathcal{H}_{\lambda\lambda'}$ maps states $\psi^{\lambda'}$ from the invariant subspace $V_{\lambda'} \subset \mathbb{C}^n$ to states ψ^{λ} from the invariant subspace V_λ. In this basis, the symmetry condition eq. (60) is equivalent to

$$\forall \lambda, \lambda' : D_\lambda(G)\mathcal{H}_{\lambda\lambda'}(G^{-1}\mathcal{K})D_\lambda^{-1}(G) = \mathcal{H}_{\lambda\lambda'}(\mathcal{K}). \tag{70}$$

Starting from this symmetry condition for each block $\mathcal{H}_{\lambda\lambda'}$ we can compute the matrix elements of the corresponding induced representation and we will find that the induced representation is a representation of $D_\lambda \otimes D^*_{\lambda'}$ acting on the space $\mathbb{C}^{n_\lambda \times n_{\lambda'}}$ where n_λ is the dimension of the invariant subspace labeled by λ. If we label the irreps in the decomposition of $D_\lambda \otimes D^*_{\lambda'}$ by the index γ we can write the blocks of $\mathcal{H}$ as:

$$\mathcal{H}_{\lambda\lambda'} = \sum_\gamma \alpha_\gamma \sum_i X_i^{(\lambda)} \mathcal{K}_l^{(\lambda')*}$$

where the $X_i^{(\lambda)}$ transform amongst themselves under the action of $D^{(X)}$ and the $\mathcal{K}_i^{(\lambda')}$ transform amongst themselves under the action of the irrep λ'. This decomposition fixes the X_is and $\mathcal{K}_i$s entirely based on the symmetry of the problem. The only freedom remaining is the choice of the values of the coefficients α_γ which are unconstrained except for the requirement that $\mathcal{H}$ must be Hermitian. In practice, these coefficients can be determined using perturbation theory.

With the theory in place, we are ready to apply it to describe holes in Germanium heterostructures. The Hamiltonian we will be working with is known as the *Luttinger-Kohn Hamiltonian*. We will describe the motivation behind the choice of basis states as well as the set of invariant matrices used to determine it in Section 4.1, but not show the invariant expansion itself, as it essentially is the same methodology as the invariant expansion of the superconductive parameter Δ which we will show in Section 4.2. For a full derivation of the Luttinger Kohn Hamiltonian we refer to [9].

4.1 Luttinger Kohn Model

So far, the subband and regular $\boldsymbol{k} \cdot \boldsymbol{p}$ methods and the envelope function approximation have expressed the Schrödinger equation in terms of the Bloch functions at zero momentum in the absence of SO interactions $u_{\nu'\mathbf{0}}$. The band index ν' runs over a discrete but infinite set, so in order to evaluate the systems of PDEs numerically we have to restrict to a finite subset of Bloch functions. The lattice of Germanium is a *diamond lattice* which possess the point group symmetry O_h. Consider a tight-binding picture of the lattice where we include an s-orbital, denoted S, and three p-like orbitals (X, Y, Z). The names s, p reference the angular momenta of these ($l = 0$ for s and $l = 1$ for p) and the angular momenta themselves a reference to which irreducible representation of $SU(2) \times C_2$ they transform under when considering a single, spherically symmetric, atom. When including the spin of the electron, the eigenstates transform according to irreducible representations

of the *double group* which are labeled by the total angular momentum j of spin and orbital motion. In the presence of other atoms in a diamond lattice, the states hybridize into bonding and anti-bonding states which are even or odd with respect to spatial inversion. Furthermore, the overall symmetry is reduced from $SU(2)\times C_2$ down to O_h. The result of this is that the subspaces labeled by j break down into invariant subspaces transforming according to the irreducible representations of subgroup O_h of $SU(2)\times C_2$. Following the notation in [24], the s-like anti-bonding states originating from a $j=\frac{1}{2}$ invariant subspace transform under the Γ_6^- irrep of O_h, where the superscript $-$ implies that these are odd under spatial inversion. The p-like anti-bonding states corresponding to $j=\frac{3}{2}$ and $j=\frac{1}{2}$ subspaces will transform under Γ_8^- and Γ_7^- respectively. Likewise for the p-like bonding states we get invariant subspaces Γ_8^+ and Γ_7^+. These invariant subspaces describe the lowest four conduction bands (Γ_8^-, Γ_7^- and Γ_6^-) and the top three valence bands (Γ_8^+ and Γ_7^+). Choosing our basis to be these 14 Bloch functions will give us the *extended Kane model*, which exactly accounts for the SO and $\boldsymbol{k}\cdot\boldsymbol{p}$ interactions between the lowest four conduction bands and the top three valence bands. $\boldsymbol{k}\cdot\boldsymbol{p}$ contributions from remote bands not included in the basis are usually accounted for using second-order perturbation theory. By performing a Schrieffer-Wolff transformation, we can reduce the size of the basis down to only include the bottom conduction band and the top three valence bands (known as the 8×8 *Kane model*) or even further down to the *Luttinger-Kohn* model which includes only the top two valence bands. We will focus on the Luttinger-Kohn Hamiltoninan in this work, so we will briefly review how to obtain the relevant invariant matrices needed in the invariant expansion of this Hamiltonian.

The 4 Bloch functions describing the top two degenerate valence bands at the Γ point form a basis for an invariant subspace V which transforms under the irrep Γ_8^+. We can express these 4 states as eigenstates of the J_z angular momentum matrix for $j=3/2$. Let $H_{LK}: V\to V$ be the Luttinger-Kohn Hamiltonian. H_{LK} is an element of a Hilbert space which is isomorphic to $V\otimes V^*$, which transforms under the product representation $\Gamma_8^+\times(\Gamma_8^+)^*$. Upon inspection of the multiplication table of the irrpes for the group O_h (see e.g. [24]) we find that:

$$V\otimes V^*\simeq V_{\Gamma_1}\oplus V_{\Gamma_2}\oplus V_{\Gamma_3}\oplus(V_{\Gamma_4}\otimes \mathbb{1}_{2\times 2})\oplus(V_{\Gamma_5}\otimes \mathbb{1}_{2\times 2}). \tag{71}$$

For each invariant subspace of $V\otimes V^*$ we can find a basis expressed in terms of the J_x, J_y, J_z. These bases are shown in Table 1. Using these bases, we can combine them with operators such as $\boldsymbol{k}, B$ and the electric field $\mathcal{E}$ (see [10] for a full list of all combinations up to fourth order in $\boldsymbol{k}$ and which irreps they belong to) such that the overall expression

Irrep	Bases	Time reversal
Γ_1:	$\mathbb{1}_{4\times4}$ or J^2	even
Γ_2:	$J_xJ_yJ_z + J_zJ_yJ_x$,	odd
Γ_3:	$\frac{1}{\sqrt{3}}(2J_z^2 - J_x^2 - J_y^2), J_x^2 - J_{y,}^2$	(even)
Γ_4:	J_x, J_y, J_z or J_x^3, J_y^3, J_z^3	odd
Γ_5:	$\{J_y, J_z\}, \{J_z, J_x\}, \{J_x, J_y\}$ or	even
	$\{J_x, J_y^2 - J_z^2\}, \{J_y, J_z^2 - J_x^2\}, \{J_z, J_x^2 - J_y^2\}$	odd

Table 1: Bases for the 4×4 matrix representation of irreducible representations of O_h. Here, $\{A, B\} = \frac{1}{2}(AB + BA)$. Adopted from [10].

will be invariant under the action of O_h. To second order in k we get:

$$H_{LK} = -\frac{\hbar^2}{2m_0}\left(\gamma_1 k^2 - \gamma_2\left[\frac{1}{3}\left(2J_z^2 - J_x^2 - J_y^2\right)\left(2k_z^2 - k_x^2 - k_z^2\right) + \left(J_x^2 - J_y^2\right)\left(k_x^2 - k_y^2\right)\right] - 4\gamma_3\left[\{J_x, J_y\}\{k_x, k_y\} + \text{c.p.}\right]\right). \tag{72}$$

Here, the coordinate directions are aligned with the main crystallographic directions in Germanium, $x\|[100], y\|[010], z\|[001]$ and can be transformed to an arbitrary different coordinate system using an isometry. The dimensionless coefficients γ_1, γ_2 and γ_3 are referred to as Luttinger parameters and are given in [10]. The two valence bands described in this Hamiltonian are known as the heavy-hole (HH) and light-hole (LH) bands on account of their different effective masses in the crystallographic z-direction, which (if neglecting off-diagonal terms) are :

$$m_z^{HH} = (\gamma_1 - 2\gamma_2)\, m_0, \qquad m_z^{LH} = (\gamma_1 + 2\gamma_2)\, m_0$$
$$m_\parallel^{HH} = (\gamma_1 + \gamma_2)\, m_0, \qquad m_z^{LH} = (\gamma_1 - \gamma_2)\, m_0$$

Note that the HH-states have *larger* in-plane effective mass than the LH-states.

Symmetry Reduction in Quasi 2D Systems

The quantum devices we aim to model in this work are Germanium heterostructures, where one direction is severely constrained compared to the other two. This added confinement inherently breaks the symmetry of the system. In the Subband $\boldsymbol{k}\cdot\boldsymbol{p}$ method we ignored this, and simply set the effective parameters in the Hamiltoninan to be the effective parameters of the bulk material but let them vary discontinuously across the interface between different materials. In terms of the theory of invariants the symmetry

Growth direction		[001]	[111]	[100]	[mmn]	[0mn]	[lmn]
inversion asymmetric z-confinement	$B_z = 0$	C_{4v}	C_{3v}	C_{2v}	C_s	C_s	C_1
	$B_z > 0$	C_4	C_3	C_2	C_1	C_1	C_1
inversion symmetric z-confinement	$B_z = 0$	D_{4h}	D_{3d}	D_{2h}	C_{2h}	C_{2h}	C_i
	$B_z > 0$	C_{4h}	C_{3i}	C_{2h}	C_i	C_i	C_i

Table 2: Point group for Germanium heterostructures depending on the growth direction and inversion symmetry of the confinement as well as the presence of magnetic fields in the growth direction. Adopted from [10].

condition Equation (60) is no longer obeyed for the point group O_h but rather some subgroup of O_h. Determining which subgroup becomes the new symmetry of the system can be done by treating the confinement as a projection onto a two-dimensional subspace of $\mathbb{R}^3$ for which the confinement direction is normal to the surface. In practice, where the quantum devices are crystallographically grown, the confinement direction is such that the two-dimensional subspace is a lattice plane. If the confinement is symmetric under inversion, the point group of the lattice plane becomes the new symmetry of the system. On the other hand, if the confinement has inversion asymmetry (if the materials above and below the quasi 2D plane are not the same for example) or the confinement potential involves a magnetic field, then the symmetry may be further reduced. The point group of a Germanium heterostructure for different growth directions is given in Table 2. If a vector space is invariant under O_h, then it is also invariant under any subgroup of O_h, and therefore, all the terms in the Luttinger-Kohn Hamiltonian, can still appear in the Hamiltonian describing the confined system. The Hamiltonian of the confined system will, however, have additional terms, and the form of these can be determined using the theory of invariants. We can use the same invariant matrices as in the Bulk case, but when combining the matrices with tensors, the combined expression does not have to transform according to Γ_1 of O_h but can transform according to different irreps of O_h as long as the expression transforms according to the Γ_1 representation of the reduced symmetry. We will focus on the case where the growth direction and the crystallographic z-direction are parallel, the z-has no magnetic field and the confinement potential is inversion symmetric. We therefore include the reduction table for the case where O_h reduces to D_{4h} in Table 3.

O_h	Γ_1	Γ_2	Γ_3	Γ_4	Γ_5	Γ_6	Γ_7	Γ_8
D_{4h}	Γ_1	Γ_3	$\Gamma_1 \oplus \Gamma_2$	$\Gamma_2 \oplus \Gamma_5$	$\Gamma_4 \oplus \Gamma_5$	Γ_6	Γ_7	$\Gamma_6 \oplus \Gamma_7$

Table 3: Conversion of the irreducible representations of the point group O_h upon confining in the crystallographic z-direction with an inversion symmetry potential and no magnetic field. Adopted from [24].

4.2 Theory of Invariants for Δ

In Section 3.1 we showed how one can determine the effective Hamiltonian describing proximitized superconductivity in the Germanium heterostructure of our system by studying the renormalized Green's function in the Germanium. If we impose symmetry constraints on the BdG Hamiltonian, we can apply the theory of invariants to obtain the allowed form of the superconductive term Δ. Imposing this symmetry constraint implicitly implies that of all the coupling terms that appear due to the presence of the superconductor, the ones that obey the impose symmetry constraint are the most dominant ones. This assumption is reminiscent of the effective mass approximation, where one assumes that the terms of highest possible (spherical) symmetry dominate over terms of lower symmetry. If one assumes that higher symmetry terms in the BdG Hamiltonian are more dominant than lower symmetry ones, then one can establish a symmetry hierarchy of Hamiltonians by gradually reducing the symmetry constraint from spherical symmetry down to the actual symmetry of the system. In this process, new terms will be added to the effective mass Hamiltonian at each reduction step. Although the underlying assumption behind this hieracical structure may not fundamentally be true, it provides a systematical and elegant way of characterizing the terms in the BdG Hamiltonian and their dependence on external fields and the wave-vector k.

In our case we use the Luttinger-Kohn Hamiltonian, H_{LK} to describe the Germanium system without superconductivity, which arose from imposing invariance under the action of O_h. We therefore impose invariance of the corresponding BdG Hamiltonian

$$\begin{pmatrix} H_{LK} & \Delta \\ \Delta^\dagger & -\Theta H_{LK} \Theta^{-1} \end{pmatrix} \tag{73}$$

under the action of O_h as well. Since the basis states of the Luttinger-Kohn Hamiltonian form an invariant subspace transforming according to the Γ_8 irrep and the set of these basis states is closed under time-reversal (i.e. if ψ is in the subspace then so is $\Theta\psi$), we see that the action of O_h on the subspace on which the BdG Hamiltonian acts is the a representation of $\Gamma_8 \oplus \Gamma_8$. From this we immediately see that Δ must also transform under $\Gamma_8 \times \Gamma_8^*$. This means that the set of invariant matrices which we can use to construct an expression for Δ is the same as the matrices used to construct the Luttinger-Kohn

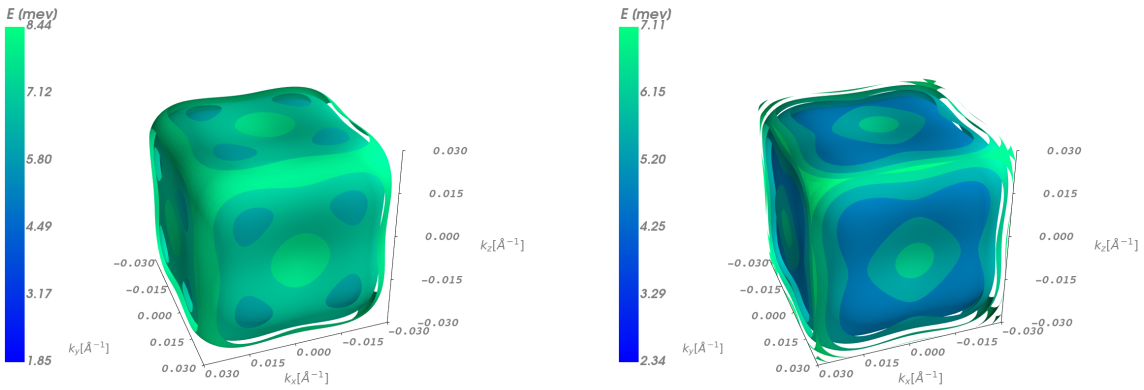

(a) $\Delta = 0$ **(b)** $\Delta = \mathbb{1} \cdot 1\text{meV}$

Figure 2: Constant energy surfaces of the lowest energy particle band of Equation (73) with chemical potential $\mu = 1.83\text{meV}$ with and without superconductive coupling Δ.

Hamiltonian. Since every term in the Hamiltonian must be invariant under the action of the symmetry (i.e. transform according to Γ_1) we must combine the matrices in Table 1 with appropriately chosen tensors $\mathcal{K}$ to achieve this. We will demonstrate this for a couple of examples and show the resulting matrix form of Δ for these as well as illustrate the dispersion relation of the extended Hamiltonian eq. (73) for different versions of Δ. However, since we will apply this theory to a Germanium heterostructure, we will mainly focus on the situation, where the symmetry is reduced from the bulk Germanium case.

Constant Δ

If we want the coupling Δ to be independent of momentum $\boldsymbol{k}$ electric field $\mathcal{E}$, and magnetic field $\mathbf{B}$, Δ must be spanned by matrices in Γ_1, which means that

$$\Delta = \alpha \mathbb{1},$$

for some $\alpha \in \mathbb{C}$. To illustrate that this choice of Δ indeed does not violate the symmetry of the Luttinger Kohn Hamiltonian, we can study the dispersion relation $E(k_x, k_y, k_z)$ for the case with $\Delta = 0$ and $\Delta \propto \mathbb{1}$. In Figure 2 we have plotted surfaces on which the LH / lowest positive-energy band of E is equal to some constant E_v. For both figures the values of E_v are the same. In a heterostructure with confinement along the crystallographic z-direction, inspection of Table 3 reveals that the two-dimensional invariant subspace Γ_3 decomposes to two one-dimensional subspaces which transform according to Γ_1 and Γ_2 respectively. The point group D_4 has 3 axes with twofold symmetry and two planes of mirror symmetry. The elements can be generated by rotations of π around each x, y and z axis and mirroring through the planes perpendicular to $x + y$ and $x - y$ respectively.

Up to a sign, these two reflections effectively swap x and y. With this, we see that one of the basis matrices of the Γ_3 subspace of O_h, $J_x^2 - J_y^2$, cannot be in the Γ_1 subspace of D_4 as it is odd under these reflections. Sine there is only one other basis vector in the Γ_3 subspace of O_h, we conclude that $2J_z^2 - J_x^2 - J_y^2$ can appear in the expression for Δ. Writing out the matrix expression for a Δ which is a linear combination of $\mathbb{1}$ and $2J_z^2 - J_x^2 - J_y^2$ in the basis of HH and LH states we find that Δ is of the form

$$\Delta = \begin{pmatrix} \alpha & 0 & 0 & 0 \\ 0 & \beta & 0 & 0 \\ 0 & 0 & \beta & 0 \\ 0 & 0 & 0 & \alpha \end{pmatrix} \tag{74}$$

where the constants $\alpha, \beta \in \mathbb{C}$ are not restricted based on symmetry. This tells us that, for the case where Δ is constant, the heavy-hole and light-hole states can have different superconductive parameters in heterostructures but not in the bulk material. Additionally, we also see that a constant Δ cannot couple LH states with HH time-reversed states in neither the bulk case nor the quasi 2D case where the confinement is along the [001] direction. Such a coupling has to involve tensor components such as $k, \mathcal{E}$ or $\boldsymbol{B}$. In Figure 3 we illustrate constant energy surfaces of the lowest particle band for a Δ which is invariant under the action of D_4 but not all of O_h. The energies defining the energy surface are the same as in Figure 2, so we can directly compare them and observe that the z-direction differs from the x and y directions in Figure 3 but not in Figure 2b.

k-dependent Δ

In the following we will look at k dependent couplings, but still keep the coupling independent of electric field and magnetic field. We start with the case where Δ is linear in $\boldsymbol{k}$. The components k_x, k_y, k_z are odd under spatial inversion, but spatial inversion is part of the O_h symmetry, so they can only appear in terms alongside quantities that are also odd under spatial inversion. Since the basis matrices or our invariant expansion are constructed from angular momentum matrices which are even under inversion, $\boldsymbol{k}$ can only appear to linear order in the expression for Δ in conjunction with either an electric of magnetic field which is inversion asymmetric. Systems which such external fields that break inversion symmetry are said to have structural inversion asymmetry (SIA), and the fact that k must appear together with an external field is a consequence of the missing bulk inversion asymmetry (BIA) in Germanium since the diamond lattice of the material has a center of inversion. A table of all SIA-type terms involving an electric field $\mathcal{E}$ up to second order in $\boldsymbol{k}$ is given in Table 4

We now move on to study the case where Δ is second order in $\boldsymbol{k}$ but independent external fields. Since terms proportional to $k_i k_j$ are even under time reversal, we only

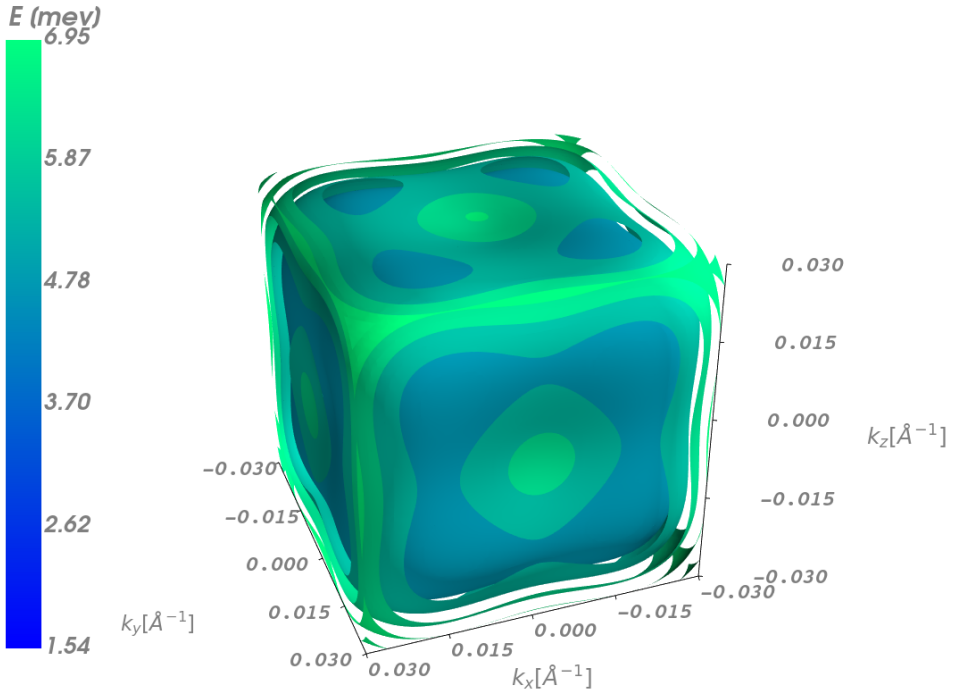

Figure 3: Constant energy surfaces of the lowest energy particle band of Equation (73) with chemical potential $\mu = 1.83\text{meV}$ and $\Delta = \left(\mathbb{1} + \left(2J_z^2 - J_x^2 - J_y^2\right)\right) \cdot 1\text{mev}$

$\Gamma_1 \times \Gamma_1$	$\nabla \cdot \mathcal{E}\ \mathbb{1}_{4\times4}$ $(\mathcal{E}_x\{k_y, k_z\} + \text{c.p.})\ \mathbb{1}_{4\times4}$
$\Gamma_3 \times \Gamma_3$	$\frac{1}{3}\left(2\{k_x, k_y\}\mathcal{E}_z - \{k_y, k_z\}\mathcal{E}_x - \{k_z, k_x\}\mathcal{E}_y\right)\left(2J_z^2 - J_x^2 - J_y^2\right) +$ $\left(\{k_y, k_z\}\mathcal{E}_x - \{k_z, k_x\}\mathcal{E}_y\right)\left(J_x^2 - J_y^2\right)$
$\Gamma_4 \times \Gamma_4$	$(\mathbf{k} \times \mathcal{E}) \cdot \mathbf{J}$ $(\mathbf{k} \times \mathcal{E}) \cdot \mathcal{J} \qquad (\mathcal{J} = (J_x^3, J_y^3, J_z^3))$
$\Gamma_5 \times \Gamma_5$	$\mathcal{E}_x\{J_y, J_z\} + \text{c.p.}$ $(k_y\mathcal{E}_z + k_z\mathcal{E}_y)\{J_x, J_y^2 - J_z^2\} + \text{c.p.}$ $(\{k_x, k_y\}\mathcal{E}_z + \{k_x, k_z\}\mathcal{E}_y)\{J_y, J_z\} + \text{c.p.}$ $(k_y^2 + k_x^2)\mathcal{E}_z\{J_y, J_z\} + \text{c.p.}$ $k_x^2\mathcal{E}_x\{J_y, J_z\} + \text{c.p.}$

Table 4: Invariant expansion terms involving an external electric field $\mathcal{E}$ up to second order in $\boldsymbol{k}$. "c.p." means cyclic permutation of the coordinates x, y, z and $\{A, B\} = \frac{1}{2}(AB + BA)$. Note that some terms have been discarded as they were not time-reversal invariant even though they did obey the spatial symmetry.

have to consider the invariant matrices that are even with respect to time-reversal:

$$\Gamma_1 : \quad \mathbb{1}_{4\times 4}, \tag{75}$$

$$\Gamma_3 : \quad \frac{1}{\sqrt{3}}\left(2J_z^2 - J_x^2 - J_y^2\right), J_x^2 - J_y^2, \tag{76}$$

$$\Gamma_5 : \quad \{J_y, J_z\}, \{J_z, J_x\}, \{J_x, J_y\} \tag{77}$$

$$\tag{78}$$

The Γ_1 case is the simplest, since it must be multiplied with a tensor which also transforms according to Γ_1 of which k^2 is the only one. For Γ_3 we have to multiply it with tensors which transform according to Γ_3 and are second order in $\boldsymbol{k}$. The following two expressions form a basis for such tensors:

$$\mathcal{K}_1 := \frac{1}{\sqrt{3}}\left(2k_z^2 - k_x^2 - k_y^2\right), \quad \mathcal{K}_2 := k_x^2 - k_y^2. \tag{79}$$

There are a total of 4 possible combinations of the basis matrices and the tensor terms, but the Γ_1 subspace is only one-dimensional, so we have to find the right linear combination of matrices and tensor terms. Based on how we know that the elements of O_h act on the spatial coordinates and the k_is, we can deduce how the representation of O_h transforms $\mathcal{K}_1$ and $\mathcal{K}_2$. We can therefore determine an explicit matrix form of the two-dimensional irreducible representation $D^{(3)}$, given by

$$D^{(3)}(g) = \begin{pmatrix}\mathcal{K}_1 \\ \mathcal{K}_2\end{pmatrix} D(g) \left(\mathcal{K}_1^\dagger \; \mathcal{K}_2^\dagger\right), \tag{80}$$

where $g \in O_h$ and D is a representation of O_h which act on the tensors. Doing the same for the two basis matrices $\frac{1}{\sqrt{3}}\left(2J_z^2 - J_x^2 - J_y^2\right), J_x^2 - J_y^2$ in place of $\mathcal{K}_1$ and $\mathcal{K}_2$ we will get exactly the same matrix expression, and by taking the tensor product $\tilde{D}(g) := D^{(3)}(g) \otimes D^{(3)}(g)$ we obtain the explicit matrix expression of the 4-dimensional representation of $\Gamma_3 \times \Gamma_3$ in the basis $\mathcal{J}_i\mathcal{K}_j$ where $\mathcal{J}_i \in \{\frac{1}{\sqrt{3}}\left(2J_z^2 - J_x^2 - J_y^2\right), J_x^2 - J_y^2\}, \quad i = 1, 2$. In this vector space we can then pick any vector $\boldsymbol{v} = \sum_{i,j\in 1,2} \alpha_{i,j}\mathcal{J}_i\mathcal{K}_j$ and compute:

$$u = \frac{1}{48}\sum_{g\in O_h} \tilde{D}(g)\boldsymbol{v}. \tag{81}$$

This u is invariant under any action of O_h since $\forall g \in O_h$:

$$\tilde{D}(g)u = \frac{1}{48}\sum_{g'\in O_h} \tilde{D}(g)\tilde{D}(g')\boldsymbol{v} = \frac{1}{48}\sum_{g''\in O_h} \tilde{D}(g'')\boldsymbol{v} = u, \tag{82}$$

where in the last step we used that $\tilde{D}$ is a group homomorphism and relabeled the summation index $g'' = gg'$. We therefore conclude that u lies in the Γ_1 subspace. Performing this computation, we find that

$$u = \frac{1}{3}\left(2k_z^2 - k_x^2 - k_y^2\right)\left(2J_z^2 - J_x^2 - J_y^2\right) + \left(k_x^2 - k_y^2\right)\left(J_x^2 - J_y^2\right). \tag{83}$$

This expression is invariant under all actions of O_h, and can therefore appear in the superconductive coupling Δ. In terms of the HH and LH states, this u takes the form

$$\begin{pmatrix} K_1 & 0 & K_2 & 0 \\ 0 & -K_1 & 0 & K_2 \\ K_2 & 0 & -K_1 & 0 \\ 0 & K_2 & 0 & K_1 \end{pmatrix}, \tag{84}$$

where $K_1 = \frac{1}{3}(2k_z^2 - k_x^2 - k_y^2)$ and $K_2 = \sqrt{3}(k_x^2 - k_y^2)$. We can take the exact same approach for the Γ_5 case, where the corresponding tensors of second order in k are

$$\{k_y, k_z\}, \{k_z, k_x\}, \{k_x, k_y\}, \tag{85}$$

which transform according to Γ_5. We find that the Γ_1 subspace in the $\Gamma_5 \times \Gamma_5$ representation is spanned by

$$\{k_x, k_y\}\{J_x, J_y\} + \{k_y, k_z\}\{J_y, J_z\} + \{k_z, k_x\}\{J_z, J_x\}, \tag{86}$$

with matrix representation:

$$\begin{pmatrix} 0 & k_z k_- & -ik_x k_y & 0 \\ k_z k_+ & 0 & 0 & -ik_x k_y \\ ik_x k_y & 0 & 0 & -k_z k_- \\ 0 & ik_x k_y & -k_z k_+ & 0 \end{pmatrix}, \tag{87}$$

where $k_\pm = k_x \pm ik_y$.

5 The Finite Element Method

With a way of constructing systems of finitely many coupled partial differential equations which can describe holes in Germanium in the presence of superconductivty, we proceed to solving these systems numerically using the *finite element method*. This method is used extensively in engineering to solve partial differential equations related to structural analysis, heat transfer, fluid flow, electromagnetism, and many more. One of the main advantages of the finite element method is that it is very capable of handling complex irregular meshes, which allows us to obtain more accurate solutions to our problem without the computational complexity becoming too great. In this section we will describe the fundamentals of the finite element method based on [25] and how we use it to obtain a (sparse) matrix representing the Hamiltonian of our problem. In Section 5.1 we then describe how to efficiently obtain a few eigenvalues and eigenstates of this Hamiltonian.

In order to keep the notation simple, we denote the system of PDEs in the following way:

$$Hu = Eu, \tag{88}$$

where H is the Hamiltonian, an $N \times N$ hermitian matrix of differential operators, u is an N-component spinor with $L^2(\Omega)$ functions defined on a bounded set $\Omega \subset \mathbb{R}^3$ as its entries, and $E \in \mathbb{R}$ is the energy. We want to only consider local solutions, so we impose that the solution must vanish on the boundary, $u(\partial\Omega) = 0$. The goal is to numerically obtain the eigenvectors u and eigenvalues E. In order to do this numerically, we have to reduce the space of functions we are working with from an infinite-dimensional Hilbert space down to a finite-dimensional one. This is done by meshing the domain Ω i.e. dividing into small but finite elements. On each of these cells we then pick a simple class of functions (in our case we choose Lagrange polynomials of order 1) and combine these into piecewise smooth functions defined on all of Ω. The set of all such functions we will call V and these functions are not differentiable at the intersection between cells, so strictly speaking they cannot be solutions to Equation (88). To overcome this, we can rephrase Equation (88) in a weaker form which allows for the possible solutions to not necessarily be differentiable everywhere. In order to do this we introduce a *trial function* $v \in \mathbb{C}_c^\infty(\Omega)$, which is a smooth function with compact support inside the domain Ω. Let $\langle \cdot, \cdot \rangle$ be the inner product on the N-component Hilbert space given by

$$\langle v, u \rangle = \int_\Omega \mathrm{d}\boldsymbol{r} \sum_{i=1}^{N} v_i^*(\boldsymbol{r}) u_i(\boldsymbol{r}). \tag{89}$$

Equation (88) implies that:

$$\langle v, Hu \rangle = E \langle v, u \rangle \quad \forall v \in \mathbb{C}_c^\infty(\Omega). \tag{90}$$

In this form, since we are working inside an integral, we can see that this equation will still make sense if u and v are not differentiable on a set of measure zero. The space of functions with this property is known as a *Sobolev space*, $H^1(\Omega)$ (for details we refer to [26]) and $V \subset H^1(\Omega)$. The weak formulation of Equation (88) is that $u \in H^1(\Omega)$ obeys

$$\langle v, Hu \rangle = E \langle v, u \rangle , \tag{91}$$

for all $v \in H^1(\Omega)$. In this form, we can approximate the Sobolev space by the finite-dimensional subspace V, that is, we search for a function $\tilde{u} \in V$ which solves Equation (91) for all $v \in V$. since V is finite-dimensional we have a basis of finitely many orthonormal vectors $\phi_j \in V$ with $j = 1, ..., N\text{dim (V)}$, so we can express $\tilde{u}$ in this basis:

$$\tilde{u} = \sum_j \xi_j \phi_j. \tag{92}$$

Inserting this into Equation (90) and picking $v = \phi_k$ we obtain $N\text{dim}V$ equations in the coefficients ξ_j which we can write as:

$$A\boldsymbol{\xi} = E\boldsymbol{\xi} \tag{93}$$

where $A_{jk} = \langle \phi_j, H\phi_k \rangle$, is hermitian because H is. For certain PDEs it is possible to prove the existence of a unique weak solution $u \in H^1(U)$ using the Lax-Milgram theorem [26] and more importantly, it is possible to show that $\tilde{u}$ will converge towards u when we make the mesh finer [25].

We have now reduced the task of approximately solving the system of PDEs as a finite-dimensional eigenvalue problem. The numerical implementation of construting the finite-element version of the PDEs is based on the FEniCSx platform [27–29] which is an open-source computing platform for solving partial-differential equation that can also run on high-performance clusters.

5.1 Efficient Partial Matrix Diagonalization

In the Finite-element method, the resulting matrix to diagonalize is sparse, and can therefore be stored efficiently, even if the size of the matrix grows very large. Furthermore, we are not interested in recovering the full spectrum but only a few states close to the Fermi surface. We therefore do not have to perform a full diagonalization, but can use iterative methods to obtain a small part of the spectrum and the corresponding eigenvectors. We will utilize the *Krylov-Schur method* [30] which is able to efficiently obtain the largest eigenvalues of a matrix. The method can also be used to determine any other part of the spectrum if it is combined with the *shift-invert*, where eigenvalues of a matrix A in the vicinity of some $\sigma \in \mathbb{R}$ are obtained by applying the Krylov-Schur method to the matrix $(A - \mathbb{1}\sigma)^{-1}$.

The main idea in the Krylov-Schur method is to project the matrix n-dimensional matrix A down to a much smaller m-dimensional *Krylov subspace* associated with A and some arbitrarily chosen vector $\boldsymbol{v}$:

$$\mathcal{K}_m(A, \boldsymbol{v}) = \text{span}\{\boldsymbol{v}, A\boldsymbol{v}, A^2\boldsymbol{v}, \ldots, A^{m-1}\boldsymbol{v}\}. \tag{94}$$

Let $H = V_m^T A V_m$ be the projection of A onto the Krylov subspace via an isomtery $V_m \in \mathbb{C}^{n\times m}$. Since H is m-dimensional, we can diagonalize it in the usual way giving us eigenvectors and eigenvalues $H\boldsymbol{v}_i = \lambda_i \boldsymbol{v}_i$. λ_i is then approximately an eigenvalue of A and $V_m^T \boldsymbol{v}_i$ is the corresponding approximate eigenvector. A measure of the accuracy of this approximation is given by the norm $\left\| AV_m^T \boldsymbol{v}_i - \lambda_i V_m^T \boldsymbol{v}_i \right\|$. The approximation is best, when V_m projects down to a subspace containing vectors which are close to eigenvectors of A. This is the motivation for projecting down to the Krylov subspace; due to the construction of $\mathcal{K}^{(m)}(A, \boldsymbol{v})$, it is very likely that the eigenvector corresponding to the largest eigenvalue will be close to this subspace, provided the initial vector $\boldsymbol{v}$ is not adversarially chosen. This approach allows us to determine some $k \leq m$ eigenvalues and eigenvectors to a certain accuracy. In order to improve the results, on can increase m, but this will increase the memory requirement of the algorithm, which potentially can lead to the algorithm failing to converge before the available memory is used up. The Krylov-Schur method therefore deflates the subspace $\mathcal{K}^{(m)}(A, \boldsymbol{v})$ down to a $p < m$ dimensional space keeping only certain eigenpairs and then extends the space by adding the Krylov subspace $\mathcal{K}^{(m-p)}(A, A^{m+1}\boldsymbol{v})$. This way, the size of the projected matrix H remains constant for each iteration, and the process of deflating and extending the space can be repeated until the desired number of eigenstates have converged to a sufficient accuracy.

The numerical implementation used to perform this partial diagonalization efficiently using the Krylov-Shur method is based on the Scalable Library for Eigenvalue Problem Computations (SLEPc) [31] which is built on the Portable, Extensible Toolkit for Scientific Computation (PETSc) [32, 33]. SLEPc is designed to solve large sparse matrix eigenvalue problems in a parallel computing setting, and therefore makes it possible to solve the diagonalization task even when the finite-element mesh is very fine.

6 Noise Sweet-Spots for Quantum Wells

In this section we will determine noise sweet spots in a gate-defined quantum dot in a Germanium heterostructure by solving the envelope function equations numerically using the finite element method. The motivation for this is that the gates defining a quantum dot are prone to noise, either as a result of cross-talk between gate electrodes or some other external factor. Due to the spin-orbit coupling, this fluctuation affects the spin degree of freedom of the hole state confined in the quantum well. Such gate noise will therefore result in dephasing of the qubit. In order to avoid this, we show that we can choose our magnetic field direction and shape of the confinement potential such that fluctuations in the confinement potential will not affect the spin. In Section 6.1 we will review the general theory of qubit dephasing and a computationally efficient method for determining the effective g-tensor known as the g-matrix formalism. In Section 6.2 we then discuss the details of modeling the quantum dot system using the methodology established in the previous sections and show the numerical results.

6.1 Qubit Dephasing and g-Matrix Formalism

In order to understand how noise in the gates defining the quantum dot can lead to a loss of information in the logical qubit, we first review the relevant theoretical aspects of qubit dephasing. We follow mainly the exposition of [34] and [35]. Since qubit dephasing is a form of loss of information, it cannot be modeled as a unitary process because unitarity implies invertibility. In the context of quantum information theory, such a process would be described by a quantum channel (a completely positive, trace-preserving map acting on the density matrices of the system) which, after "going to the church of the larger Hilbert space", can be modeled as a unitary operation on a larger Hilbert space describing both the qubit and the environment that it interacts with (This is a special case of Stinespring's dilation theorem [36]). The final mixed state of the qubit is then determined by summing over all degrees of freedom in the environment using a partial trace. Instead of fixing a specific model for the environment and its interactions with the qubit, we will simply treat the bath as a classical noise process which is sufficient for our purposes. The magnetic field applied to the quantum well splits the spin degree of freedom of the hole state which encodes our qubit. The Hamiltonian describing the time-evolution of our two-level system can be written as:

$$H = \frac{\hbar}{2}\omega_0\sigma_z$$

where σ_z is the Pauli z-matrix. ω_0 describes the energy splitting of the two spin states as a result of the $\boldsymbol{B}$ field so it depends on the effective g-factor. Due to fluctuations in the confinement potential, the effective g-factor fluctuates over time, which in turn affects the level splitting by altering ω_0. We can model this fluctuation by replacing ω_0 by a classical random variable that fluctuates by $\delta\omega(t)$ in time around ω_0. We will assume that this random variable is such that it averages to the zero-function i.e. $\langle\delta\omega(t)\rangle = 0$. Experimentally, this averaging over different noise functions would correspond to averaging the noise over different devices or, if the noise is time-dependent, averaging over multiple runs. Plugging this into the Hamiltonian we have,

$$H = \frac{\hbar}{2}(\omega_0 + \delta\omega(t))\sigma_z. \tag{95}$$

Due to the difference in energy, time-evolution of the quantum states adds different phase factors:

$$U(t) = \begin{pmatrix} e^{i\phi(t)/2} & 0 \\ 0 & e^{-i\phi(t)/2} \end{pmatrix}, \tag{96}$$

with $\phi(t) = \omega_0 t + \int_0^t \mathrm{d}t'\delta\omega(t')$. The density matrix of the system as a function of time then becomes:

$$\rho(t) = U(t)\rho(0)U^\dagger(t) = \begin{pmatrix} \rho_{11} & \rho_{10}e^{i\phi(t)} \\ \rho_{01}e^{-i\phi(t)} & \rho_{00} \end{pmatrix}, \tag{97}$$

where ρ_{ij} are the components of the initial density matrix at time $t = 0$. Assuming now that the phase $\phi(t)$ is distributed according to a Gaussian distribution with mean $\langle\phi(t)\rangle = \omega_0$ (since $\langle\delta\omega\rangle = 0$) and variance $\langle\phi^2(t)\rangle = \left\langle \left(\int_0^t \mathrm{d}t'\delta\omega(t')\right)^2 \right\rangle$ we can compute the expectation value of the density matrix (with expectation taken over all possible noise functions $\delta\omega$)

$$\langle\rho(t)\rangle = \begin{pmatrix} \rho_{11} & \rho_{10}\left\langle e^{i\phi(t)}\right\rangle \\ \rho_{01}\left\langle e^{-i\phi(t)}\right\rangle & \rho_{00} \end{pmatrix} = \begin{pmatrix} \rho_{11} & \rho_{10}e^{i\omega_0 t}e^{-\left\langle\phi^2(t)\right\rangle/2} \\ e^{-i\omega_0 t}e^{-\left\langle\phi^2(t)\right\rangle/2} & \rho_{00} \end{pmatrix}. \tag{98}$$

Since noise tends to not cancel itself over time, $\langle\phi^2(t)\rangle$ will be an increasing function in time, which implies an exponential decay in the off-diagonal terms. Hence, if the initial state was pure it will tend to a mixed state over time.

This shows that fluctuations in the confinement potential lead to qubit dephasing by varying the effective g-factor which results in fluctuations of the energy splitting of the qubit states. We therefore study the effects of the gate noise on g-factor as a function of the parameters defining the gate, in order to determine how to eliminate this source of dephasing. In Germanium the g-factor is anisotropic, and we therefore need to describe it as a tensor. If we can determine the g-tensor and how it behaves when the potentials are varied, we can use this to determine which magnetic field directions and confinement

configurations give the lowest possible fluctuations of the energies when the confinement potential fluctuates. The entire g-tensor can be efficiently computed from the eigenstates at zero magnetic field using the g-matrix formalism [37], which we will briefly describe here.

The EFA Hamiltonian with added magnetic field $\boldsymbol{B}$ and confinement potential Vcan be written as:

$$H = H_0 + \boldsymbol{M} \cdot \boldsymbol{B} + \mathcal{O}\left(\boldsymbol{B}^2\right), \tag{99}$$

where H_0 is an operator and $\boldsymbol{M}$ is a vector with operators as entries, all of which are independent of $\boldsymbol{B}$. We will ignore the higher order contributions of $\boldsymbol{B}$ and write the lowest eigenstates to H_0 as $|\Uparrow\rangle$ and $|\Downarrow\rangle$:

$$H_0 |\Uparrow\rangle = E_0 |\Uparrow\rangle, \quad H_0 |\Downarrow\rangle = E_0 |\Downarrow\rangle. \tag{100}$$

In the subspace spanned by this Kramer's pair, we find that the matrix expression for H is:

$$\langle \sigma \mid H \mid \sigma' \rangle = \delta_{\sigma\sigma'} E_0 + \langle \sigma \mid \boldsymbol{M} \mid \sigma' \rangle \cdot \boldsymbol{B}, \tag{101}$$

where $\sigma, \sigma' \in \{\Uparrow, \Downarrow\}$. In the second term, the matrix expressions for M_x, M_y and M_z can be expressed as a linear combination of Pauli-matrices σ_x, σ_y and σ_z (The magnetic field term must split the Kramer's degeneracy, so a term involving $\mathbb{1}$ in the expression for the M_is cannot appear). Specifically, the general form of the second term can be written as:

$$\frac{1}{2}\mu_B \boldsymbol{\sigma}^T \hat{g} \boldsymbol{B}, \tag{102}$$

where $\hat{g}$ is the g-matrix, a 3×3 matrix of real entries. Comparing this expression with Equation (101) we see that the elements of $\hat{g}$ are:

$$\hat{g} = \frac{2}{\mu_B} \begin{pmatrix} \Re\left(\langle\Downarrow| M_x |\Uparrow\rangle\right) & \Re\left(\langle\Downarrow| M_y |\Uparrow\rangle\right) & \Re\left(\langle\Downarrow| M_z |\Uparrow\rangle\right) \\ \Im\left(\langle\Downarrow| M_x |\Uparrow\rangle\right) & \Im\left(\langle\Downarrow| M_y |\Uparrow\rangle\right) & \Im\left(\langle\Downarrow| M_y |\Uparrow\rangle\right) \\ \langle\Uparrow| M_x |\Uparrow\rangle & \langle\Uparrow| M_y |\Uparrow\rangle & \langle\Uparrow| M_z |\Uparrow\rangle \end{pmatrix}. \tag{103}$$

This $\hat{g}$-matrix can be transformed to the conventional symmetric form of the g-tensor upon a change of basis of the x,y and z directions as well as a unitary transformation of the ground state Kramer's pairs $|\Uparrow\rangle$ and $|\Downarrow\rangle$. From a single evaluation of the ground state of the H_0 we can determine the Zeeman splitting of these for any magnetic field:

$$H_{\text{Zeeman}} = \frac{1}{2}\mu_B g^* \|\boldsymbol{B}\| \, \boldsymbol{u} \cdot \boldsymbol{\sigma}, \tag{104}$$

where the effective g-factor $g^* = \|\hat{g}\boldsymbol{B}\| / \|\boldsymbol{B}\|$ and $\boldsymbol{u} = \hat{g}\boldsymbol{B}/\|\hat{g}\boldsymbol{B}\|$ is a unit vector. The dependence of the confinement potential V is implicit in the states $|\Uparrow\rangle, |\Downarrow\rangle$ as they are solutions to H_0 which depends on V. The g-matrix formalism therefore allows us to study the dependence of g^* as a function of the confinement potential V efficiently using very few numerical evaluations of the eigenstates of the envelope function Hamiltonian.

6.2 Implementation and Numerical Results

Our envelope function Hamiltonian is the Luttinger-Kohn Hamiltonian described in Section 4.1,

$$H_{LK} = \frac{\hbar^2}{2m_0}\left(\gamma_1 k^2 - \gamma_2\left[\frac{1}{3}\left(2J_z^2 - J_x^2 - J_y^2\right)\left(2k_z^2 - k_x^2 - k_z^2\right) + \left(J_x^2 - J_y^2\right)\left(k_x^2 - k_y^2\right)\right]\right. \\ \left. - 4\gamma_3\left[\{J_x, J_y\}\{k_x, k_y\} + \text{c.p.}\right]\right). \tag{105}$$

Note that we have removed a minus sign to make the dispersion particle-like, which will make discussion easier when we add time-reversed states later. We will set the growth direction of the heterostructure to be the z-direction (crystallographic axis [001]) and the total width of the infinitely deep well potential is set to $L_z := 25\text{nm}$ in accordance with recent experiments [6, 7] as wells as the Germanium heterostructures constructed at the Center for Quantum Devices at the University of Copenhagen.

Performing the subband $k \cdot p$ method amounts to evaluating the k_z and k_z^2 for the plane-wave solutions Equation (12), for which we get:

$$\langle n \mid k_z \mid m\rangle = -i\frac{nm}{(n^2 - m^2)L_z}((-1)^{n+m} - 1), \quad \left\langle n \mid k_z^2 \mid m\right\rangle = \delta_{nm}\frac{\pi^2}{L_z^2}. \tag{106}$$

The most dominant contribution of this comes from the diagonal elements of k_z^2 which, because of the strong confinement, removes the degeneracy of the HH and LH-states at $\boldsymbol{k}_\parallel = 0$, due to the different effective masses of these bands. This observation is also consistent with the fact that the added potential breaks the O_h symmetry of the problem, so the 4-dimensional Γ_8 subspace decomposes into two lower-dimensional subspaces (In this case the symmetry is reduced to the point group D_{4h} and Γ_8 decomposes to the invariant subspaces Γ_6 and Γ_7). Furthermore, the strong confinement means that the energy difference between the lowest z-mode and any excited mode n scales as $\mathcal{O}\left(n^2 L_z^{-2}\right)$. This suggests that not very many modes m need to be considered in order to obtain a good approximation of the lowest HH band. In fact, judging from the dispersion in Figure 4, it is already a reasonable approximation to only consider the lowest energy z-mode, which effectively just shifts the HH and LH bands upwards by $\hbar^2\pi^2/(2L_z^2 m_z)$ which evaluates to 2.95meV for the HH band and 13meV for the LH band.

We assume that the magnetic field applied to the system is weak enough so that we can neglect its effect on the orbital motion, so we ignore the vector potential $\boldsymbol{A}$ and only add a $\boldsymbol{B}$ field. In terms of the Luttinger Kohn Hamiltonian, terms involving $\boldsymbol{B}$ must be invariant under the symmetry operations of the system. Since $\boldsymbol{B}$ transforms like an axial vector and is odd under time-reversal, it follows that $\boldsymbol{B}$ transforms according to Γ_4, and must therefore be multiplied with matrices transforming according to Γ_4 as well. The resulting terms are:

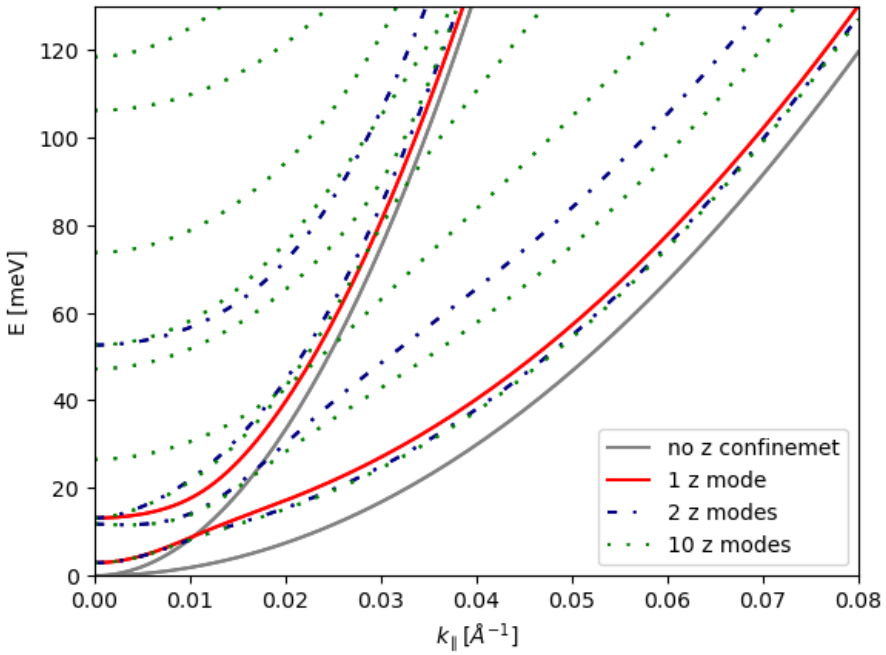

Figure 4: In-plane dispersion of the Luttinger-Kohn Hamiltonian for Germanium both with and without a 25nm wide infinite well potential in the [001] direction. The dispersion with z-confinement is shown for different numbers of z modes included in the matrix.

$$H_B = \mu_B \left[\kappa \boldsymbol{J} \cdot \boldsymbol{B} + q' \mathcal{J} \cdot \boldsymbol{B}\right] \tag{107}$$

where $\boldsymbol{J}$ is a vector of the $j = \frac{3}{2}$ angular momentum matrices, J_i and $(\mathcal{J})_i = J_i^3$. The dimensionless coefficients κ and q are given in [10]. The confinement potential chosen is a simple harmonic oscillator $V(\boldsymbol{r}) = \frac{1}{2} m_0(\omega_x^2 x^2 + \omega_y^2 y^2)$. In order to investigate the variation of the effective g-factor when the shape of this potential changes, we fix ω_y and vary ω_x. For each cell in the finite-element mesh, we choose to express the functions as Lagrange polynomials of order 1, which essentially means that the resulting eigenstates will be piecewise linear functions. Figure 5 shows one of the states of the ground state Kramers pair for a few specific configurations of the potentials and Figure 6 shows how the changes in the confinement potential shape affect the singular values of the g-matrix which correspond to the principal g-factors. The corresponding principal magnetic field directions are the the z-axis for the g_3 component, the x-axis for the component which increases as a function of ω_x and the y axis for the remaining component. This shows that increasing the confinement in the x-direction also increases the g-factor in that direction while decreasing the g-factor in the other directions. This difference in the behaviour of the tensor components means that there exist $\boldsymbol{B}$-fields for which $\|\hat{g}\boldsymbol{B}\|$ is unchanged under fluctuations of the confinement potential. To leading order, the fluctuation can be

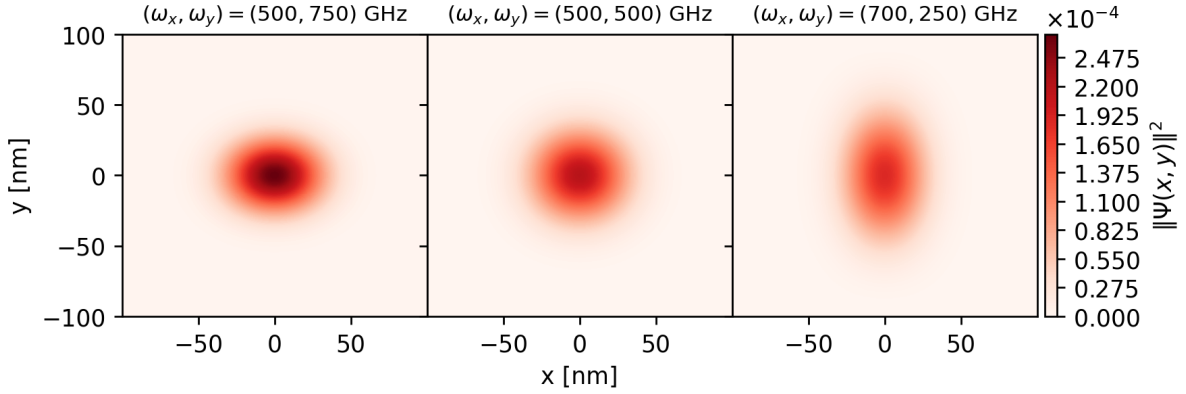

Figure 5: Positional probability distributions of the ground state wave function for different confinement potentials.

expressed by replacing $\hat{g} \to \hat{g} + \delta\hat{g}$. Doing so, the effective g-factor becomes

$$\frac{1}{\|\boldsymbol{B}\|}\|\hat{g}\boldsymbol{B}\| \to \frac{1}{\|B\|}\|\hat{g}\boldsymbol{B}\| + \frac{1}{\|\boldsymbol{B}\|\,\|\hat{g}\boldsymbol{B}\|}(\hat{g}\boldsymbol{B})^T\delta\hat{g}\boldsymbol{B} + \mathcal{O}\left(\delta g^2\right). \tag{108}$$

From this we see that the fluctuation in the effective g-factor vanishes if we choose $\boldsymbol{B}$ such that $\hat{g}\boldsymbol{B}$ and $\delta\hat{g}\boldsymbol{B}$ are orthogonal. The qualitative trend of g-tensor components when changing ω_x does not appear to be an artifact of the discretization of the PDEs, since Figure 6 also shows that making the mesh finer results in insignificant changes to the values. The big difference between the in-plane and out of plane g-factors are a result of the strong confinement in the z-direction and the values are similar to what has been observed in experiments [6]. As an extra confirmation that the assumptions used in the g-matrix formalism are valid for this system, we compare the predicted Zeeman splitting of the ground state Kramers pair, $\Delta E = \mu_B\|\hat{g}\boldsymbol{B}\|$ to the actual computed energy splitting for some randomly chosen confinement potentials ω_x, ω_y and magnetic fields $\boldsymbol{B}$ of strength 100mT. The relative error between the results was around 10^{-6} so we conclude that the g-matrix formalism is valid for this system. While modeling the confinement potential as a harmonic oscillator potential is by no means the most accurate description of a quantum dot, we believe that it still establishes the existence of a sweet spot where quantum dots can be made resistant towards gate noise fluctuations. The numerical implementation used to produce these results is capable of handling more involved descriptions of the confinement potential, and can therefore potentially be used to look for sweet spots for a specific device architecture, and be used to aid the design of noise robust devices. The code used in this project is built to allow for parallel computing, both when assembling the Hamiltonian and when performing the partial matrix diagonalization afterwards. The code is therefore capable of modeling systems to a level of detail beyond what would be feasible on a single computer.

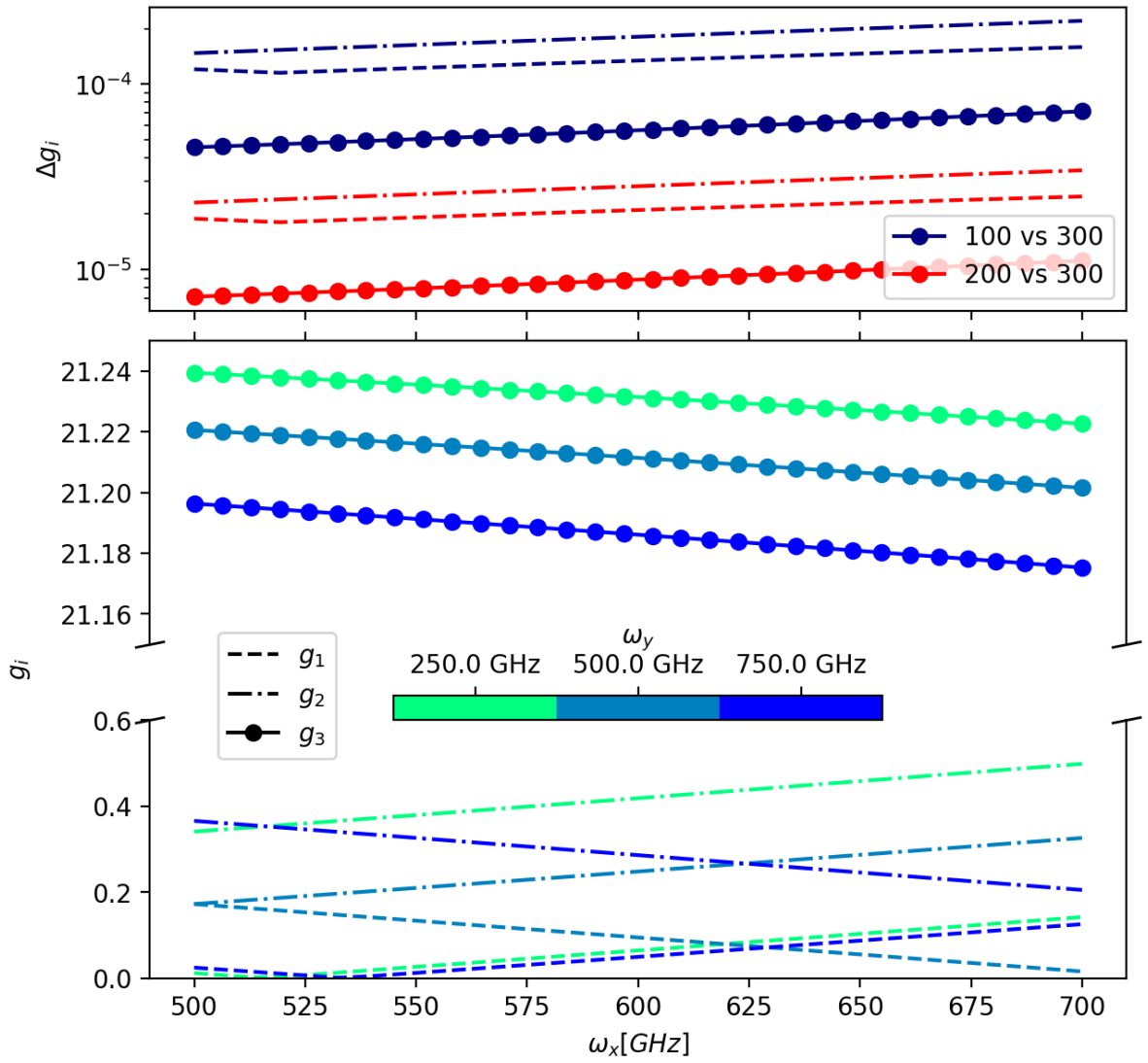

Figure 6: Bottom: Singular values of the g-tensor as function of confinement in the x-direction for three different y confinements.
Top: Average difference of singular values of the g-tensor for different resolutions of the finite element mesh. The meshes studied were generated by partitioning each of the in-plane directions into 100,200 and 300 cells.

7 Superconductor Mediated Coupling of Quantum Dots

We now shift our attention to studying the coupling of quantum dots through a superconductor. The goal is to investigate how the regular tunnel coupling and the cross Andreev reflection (CAR) depend on parameters of the system such as the chemical potential in the superconductor and length of the superconductor. In addition, we study how spin orbit contributes to the coupling. In a simple, illustrative model of the system we can think of the two quantum dots as two coupled two-level systems. The Hamiltonian for such a system is:

$$H = \begin{pmatrix} \varepsilon_L + B & 0 & 0 & 0 & t & t_{SO} & \Delta_{SO} & \Delta \\ 0 & \varepsilon_L - B & 0 & 0 & t_{SO} & t & \Delta & \Delta_{SO} \\ 0 & 0 & -\varepsilon_L - B & 0 & -\Delta_{SO} & -\Delta & -t & -t_{SO} \\ 0 & 0 & 0 & -\varepsilon_L + B & -\Delta & -\Delta_{SO} & -t_{SO} & -t \\ t & t_{SO} & -\Delta_{SO} & -\Delta & \varepsilon_R + B & 0 & 0 & 0 \\ t_{SO} & t & -\Delta & -\Delta_{SO} & 0 & \varepsilon_R - B & 0 & 0 \\ \Delta_{SO} & \Delta & -t & -t_{SO} & 0 & 0 & -\varepsilon_R - B & 0 \\ \Delta & \Delta_{SO} & -t_{SO} & -t & 0 & 0 & 0 & -\varepsilon_R + B \end{pmatrix}. \quad (109)$$

In this matrix, the top left 4×4 block describes the on-site energies of the left dot where both the particle states and time-reversed states are included. B (in units of energy) is an external magnetic field splitting the spin-states into non-degenerate states. Similarly, the lower 4×4 block describes the on-site energies in the right dot. The off-diagonal blocks describe the coupling between two dots. The coupling terms denoted by t are related to the tunneling process where a particle / anti-particle can tunnel from one dot to the other. In the presence of spin-orbit coupling, it is possible that the spin is flipped during this process, which is why we have included coupling coefficients t_{SO} in the Hamiltonian. The other coupling mechanism of the dots is related to the superconductor's coupling of particles and anti-particles. These terms are labeled with Δ and correspond to the process where a particle from one dot enters the superconductor, combines with another particle of opposite spin to form a Cooper pair and the extra 'hole' created in the process exits into the other dot. Spin-orbit coupling during this process allows the spin to flip during this process as well so we also include Δ_{SO}. In practice, the on-site energies and B will be so that all these 8 states lie closer to the chemical potential than the superconductive gap. When numerically solving the envelope function model of this system, we therefore simply need to compute the eigenenergies closest to the chemical potential to effectively obtain the eigenvalues of Equation (109). Based on these eigenvalues, we want to determine the

coupling coefficients Δ and t. One way to approach this, is to look for avoided crossings when varying ε_L and ε_R. If we ignore the magnetic field and set ε_L and ε_R to be some $E_0 > 0$ which is larger than $|t|$ and $|\Delta|$ (with the energy scale set so that $\mu = 0$), then the left and right particle states will hybridize into bonding and antibonding states split by $2|t|$. The same thing occurs for the anti-particle states. If we, on the other hand, fix ε_L to E_0 and ε_R to $-E_0$ the particle states of the right dot hybridize with the anti-particle states in the right dot to form bonding and antibonding states which are split by $2|\Delta|$.

In Figure 7 these avoided crossings are illustrated by using a 1D tight-binding model of the dot-superconductor-dot. In this model, each site comprises simply a particle state and an anti-particle state (so the spin degree of freedom is ignored). The left and right ends of the chain are the left and right dots with on-site energy ε_L and ε_R respectively. There is a regular hopping term from the dot-sites to the closest neighboring site which adds coupling terms between particle states on the neighboring sites and similarly for anti-particle states. For all states except the dot states, there is also a superconductive term coupling particle states at one site to the anti-particle states at the same site. The on-site energy of the states describing the superconductor (which provides a description of the chemical potential in the superconductor) is chosen such that there is a mixing of particle and anti-particle states (i.e. the band is partially filled). Fixing some E_0 such that there will be 4 in-gap states when $(\varepsilon_R, \varepsilon_L) = (E_0, E_0)$, we can see the avoided crossings when we vary ε_L and ε_R a little around the points $(\varepsilon_L, \varepsilon_R) \in \{(E_0, E_0), (E_0, -E_0), (-E_0, -E_0)(-E_0, E_0)\}$.

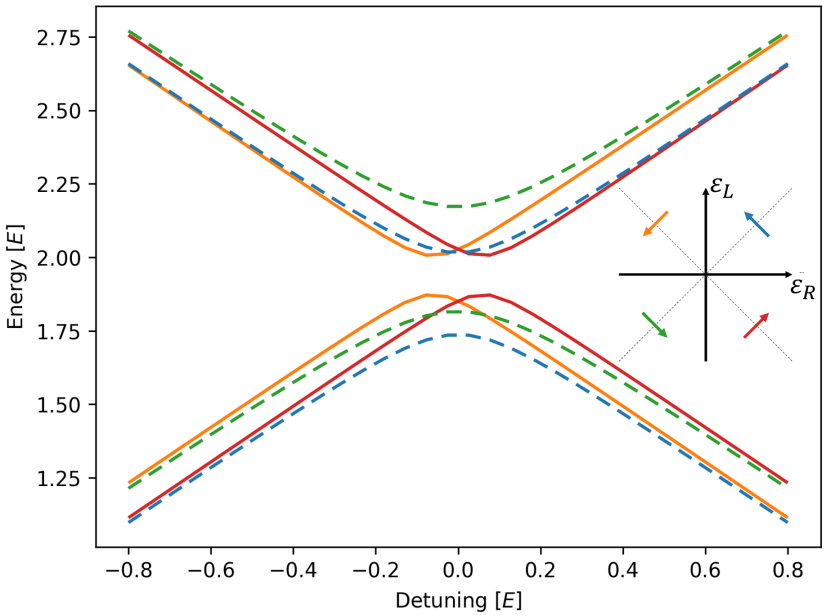

Figure 7: Positive energy in-gap states for the 1D tight-binding model for the dot-superconductor-dot system as a function of detuning. The arrows in the inset indicate the direction of increasing detuning.

Finite-Element Model Construction

Similarly to the 1D case, this methodology for determining t and Δ can be applied to the finite-element system as well. First we must define the model for the dot-superconductor-dot system. Just as in Section 6 the z-confinement is chosen to be 25nm and we can therefore also in this case neglect higher orbital excitations in the z-direction. As for the form of the superconductive parameter Δ, we chose it simply proportional to the identity; although we could in principle choose different superconductive couplings for the heavy-hole and light-hole states without violating the symmetry of the quasi-2D system as discussed in Section 4.2. Due to the large energy splitting of the HH and LH bands caused by the z-confinement, the chemical potential in the superconductor has to be chosen significantly larger than in the dots in order for the HH-band to become populated. We therefore argue that the details of the superconductive coupling of the LH states is not important and we are free to choose it to be the same as to superconductive coupling of the HH states.

The potential surface defining the quantum dots and the superconductor is constructed by a piecewise combination of potentials constructing the individual components. Each dot is modeled as a potential of the form $\tilde{V}_L(\boldsymbol{r}) = \frac{1}{2}m_e\omega_0^2(\boldsymbol{r}-\boldsymbol{r}_L)^2 + \frac{C}{4}(\boldsymbol{r}-\boldsymbol{r}_L)^4 + V_L$ where $\boldsymbol{r}_L$ is the center of the left dot and the constant V_L is added to allow for adjusting the energy of the states localised in the left dot. The potential defining the right dot is defined analogously, and the constants ω_0 and C are the same for both dots. The superconductor is simply a rectangular region with constant potential V_{SC} and non-zero superconductive coupling Δ. At the interface between the superconductor and a dot, there is a region of constant potential V_B and no superconductive coupling acting as a barrier potential. For the eigenstates of the system, initial runs with a coarse, uniform mesh show that the wave function in the dots appears Gaussian and oscillates rapidly in the superconductor. Based on this observation we chose to construct a mesh which is finer inside the superconductor than in the dots. Around the barrier between the dots as well as in the center of the dots the resolution is also increased, as we expect the gradient of the eigenstates to vary more in these areas. The mesh and an example potential surface is shown in Figure 8a and Figure 8b shows two eigenstates of system defined by the example potential.

In the finite-element model, we can vary the energy in the dots using a constant potential in each dot, V_L and V_R. When the potential in both dots is the same ($V_L = V_0 = V_R$), their energy will be equal, and we can determine the t-coupling by letting $V_L = V_0 + \epsilon$ and $V_R = V_0 - \epsilon$ for some small ϵ and minimizing the energy difference between the lowest energy hole states (ignoring spin degeneracy) as a function of ϵ. When varying V_L the coupling to the superconductor changes, and as a result, it is difficult to determine the point where the hole states in the right and left dot have exactly the same

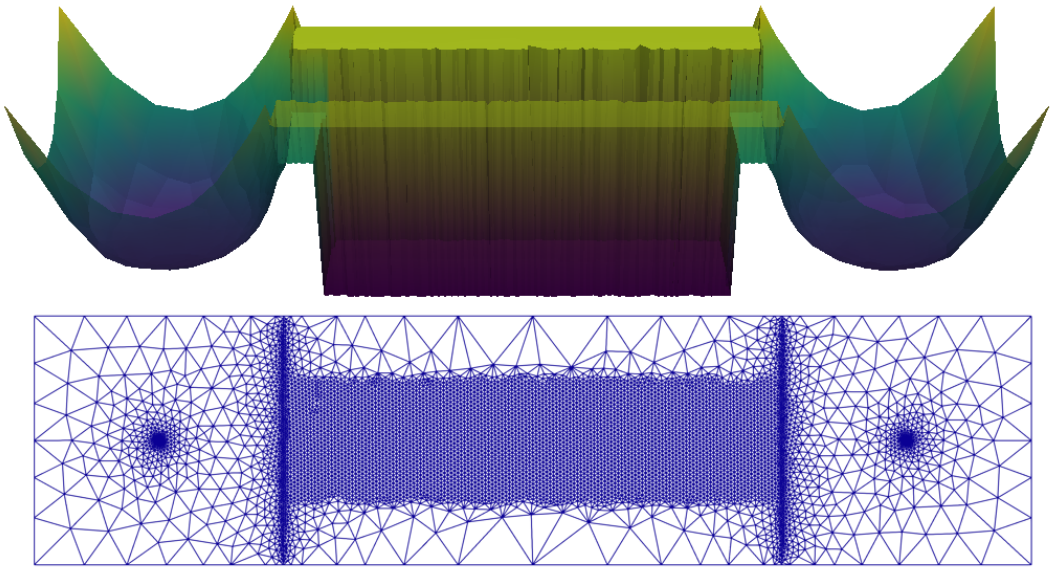

(a)

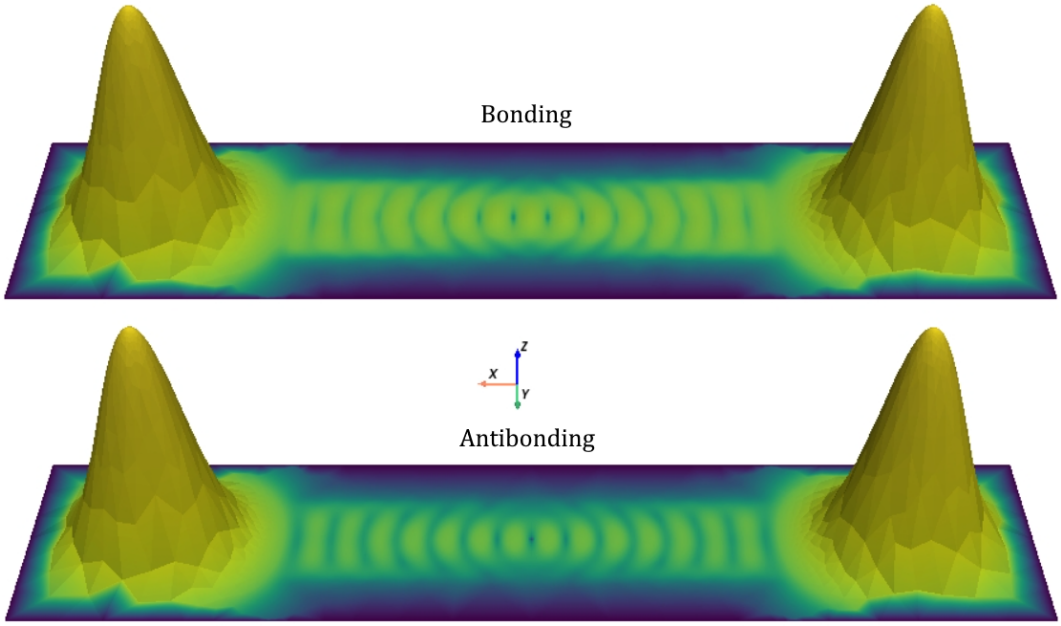

(b)

Figure 8: (a) Example potential describing the dot-superconductor-dot system. The potential is interpolated on the mesh shown, which is the same mesh used in the finite element computation.
(b) Two of the 8 in-gap eigenstates of the system described by the potential shown in (a). The z axis represents the norm $\|\psi(x,y)\|^2$ scaled such that it takes values from 0 to 1. The coloring also illustrates $\|\psi(x,y)\|^2$ but on a log scale to better illustrate the wave function in the superconductor where the amplitude is orders of magnitude lower than the amplitude in the dots.

distance to the Fermi surface, but are on different sides. Therefore, we determine Δ in the following way: let $V_L = V_0 = V_R$ and determine the ground state hole energy, E_{GS}. Set $V_L = V_0 - E_{\text{GS}} + \epsilon$ and minimize energy difference between the lowest energy states (again ignoring spin degeneracy) as a function of ϵ. These minimization tasks can be computed efficiently in terms of the number of times the envelope function model has to be solved since our initial guesses for V_L and V_R put us close enough the the global minimum so that minimization will not get stuck in a local minimum. In practice, we find that it takes around 15 evaluations of the envelope function model to determine the minima within numerical precision. In fact, for the case where the left and the right dots are identical, the minimum determining the t coupling will always be when $V_L = V_R$ so in this case, it is not necessary to perform the minimization. This minimization only determines the magnitude of the couplings, but gives no information about the sign. The sign can be deduced from inspecting the ground state wave-function. For the case where t is to be determined, The wave-function is either symmetric or anti-symmetric when reflecting through the middle of the superconductor. If the ground state is symmetric, the tunnel coupling is attractive, i.e. $t > 0$, and if the ground state changes sign under reflection the tunnel coupling is repulsive ($t < 0$). For the CAR coupling, the sign of Δ can be determined in a similar fashion, but the symmetry operation in this case is a reflection through the middle of the superconductor **and** an interchange of the particle and anti-particle components.

Figure 9 shows the tunnel and CAR couplings of two identical dots as a function of the chemical potential in the superconductor as well as the strength of the superconductive coupling. t and Δ change sign at the points where they go to 0, and the points where both couplings become large are roughly where the Fermi wave-vector in the superconductor obeys: $k_f L_{\text{SC}} = \pi$. We see the same behaviour for different lengths of the superconductor, but the couplings generally increase as the length of the superconducutor is reduced. This method provides a computationally inexpensive way of determining the couplings of the two dots, and if an external magnetic field is applied to split the degeneracy of the spin-states in the dots, one could also gain insight into how spin-orbit interaction affects these couplings. In experimental settings, the energy levels in the dots will be somewhat close to the Fermi surface. As our methodology relies on having only two states being close in energy, we expect that this method will not work well when the states are very close to the Fermi surface. In the regime where the dots are close to the Fermi surface, more of the wave-function for the in-gap states will also leak into the superconductor. As a result of this, one can no longer ignore what is going on inside the superconductor, so the fundamental assumption behind the effective Hamiltonian eq. (109) of describing the system as two coupled dots breaks down. One way of illustrating this, is to let $V_L = V_R =: V$ and plot the in-gap energies as a function of V. This is done in Figure 10.

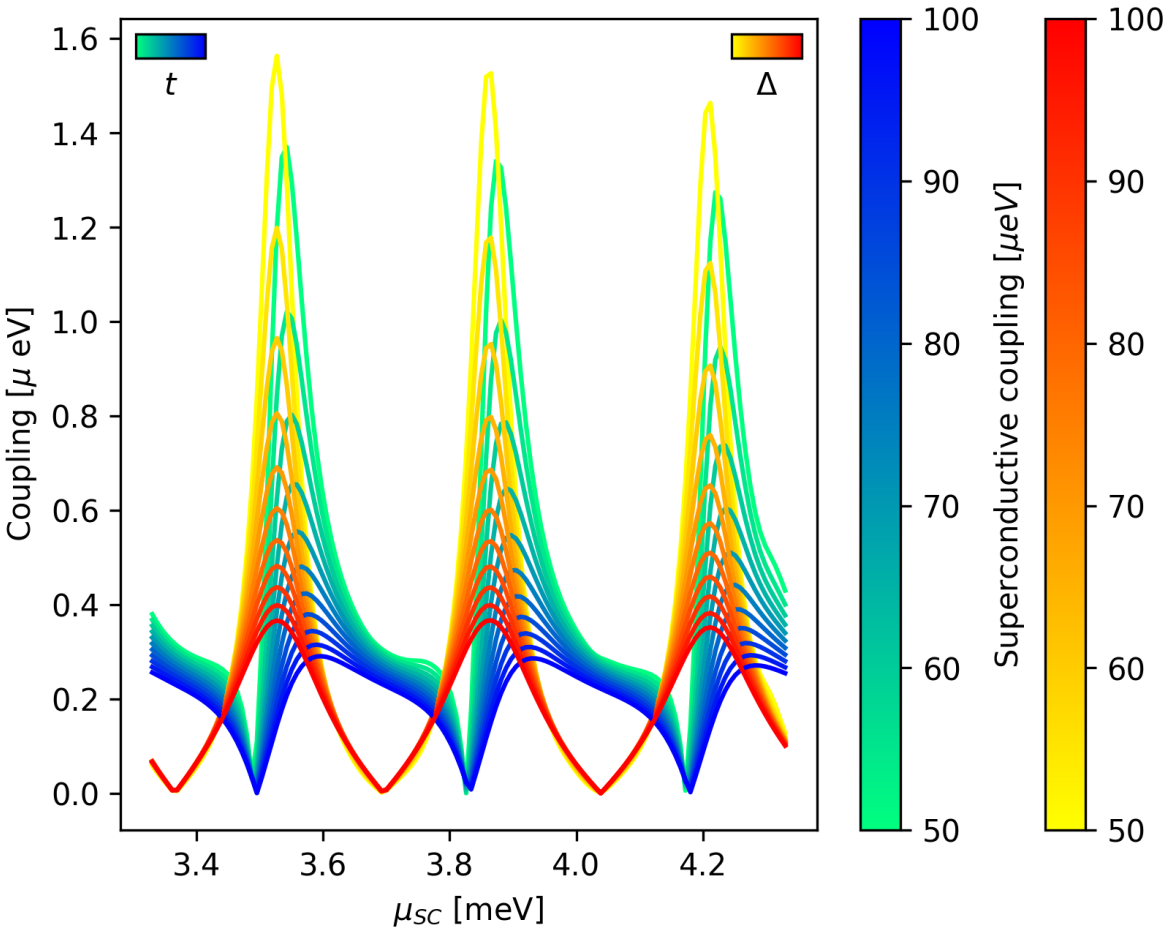

Figure 9: Coupling coefficients t and Δ as functions of the chemical potential and the strength of the superconductive coupling in the superconductor. Determined using the finite-element model.

When the potential is small, the 4 negative energy states are particle-like and are grouped into two two-fold degenerate eigenspaces corresponding to symmetric and anti-symmetric orbital wave-functions. The 4 positive energy eigenstates are anti-particle-like and also group into symmetric and anti-symmetric states. The splitting of the symmetric and anti-symmetric particle states matches the t coupling coefficient, so in this regime, the model Hamiltonian eq. (109) is accurate. As the potential in the dots increases and the eigenstates approach the Fermi surface the symmetric and anti-symmetric states exhibit different avoided crossings. For large V the negative energy states are anti-particle-like and the positive energy states are particle-like. In this limit, the t coupling between the symmetric and anti-symmetric states is smaller. These phenomena do not fit with the model Hamiltonian eq. (109). The simplest way to see this, is to notice that the spectrum $\sigma(H)$ is unchanged when switching the sign of the dot energies $\varepsilon_L, \varepsilon_R \to -\varepsilon_L, -\varepsilon_R$. This

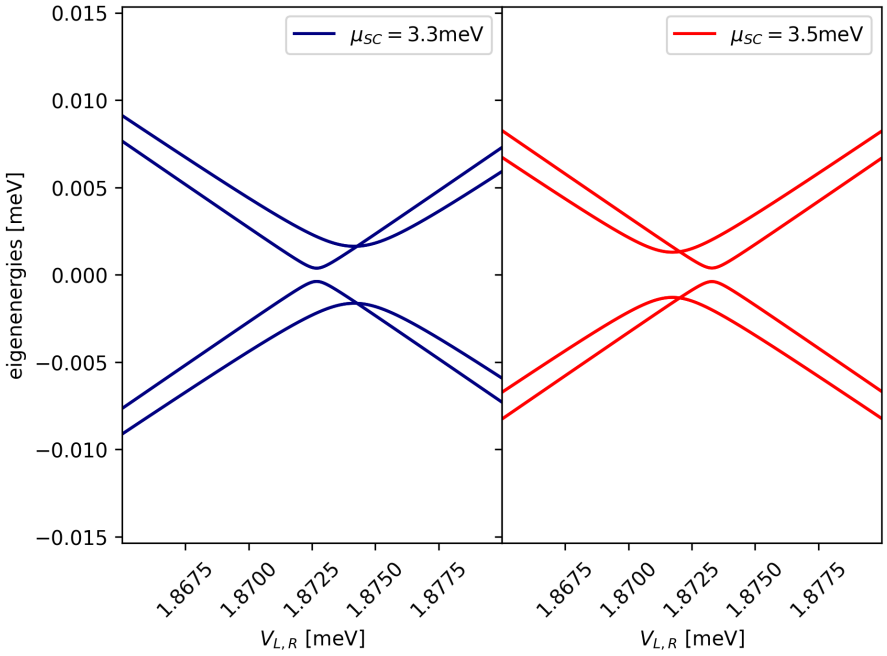

Figure 10: All 8 in-gap eigenenergies of the FE-modeled dot-superconductor-dot system as a function of the potential in the dots. Shown for two specific values of the chemical potential in the superconductor.

model therefore implies that the spectrum must be symmetric around some specific value of the dot potential, which is not the case. The apparent asymmetry that we observe when 'flipping the sign' of the dot energies by increasing the potential comes from the interaction between the dots and the superconductor. Since we keep the parameters specifying the superconductor constant throughout, the coupling between the superconductor and the dots does not stay the same when increasing the dot potential. If we were to also 'flip' the spectrum of the superconductor, then we would reestablish the symmetry. We can directly verify this argument using the 1D tight-binding model, where we can easily change the sign of the on-site energy in the superconductor. Figure 11 shows that the spectrum is unchanged when flipping the on-site energy both in the superconductor as well as in the dots. This symmetry is essentially the particle-hole symmetry of the Bogoliubov-de Gennes equations.

The second phenomenon which is not captured by the simple model, is the different coupling of the symmetric and anti-symmetric particle / anti particle states. Further inspection of the wave functions reveals that the state with higher coupling to its time-reversed counterpart it the one which also has more weight within the superconductor. Whether the state with higher weight in the superconductor is symmetric or anti-symmetric depends on the chemical potential in the superconductor, or more specifically, the fermi-wave vector. We can demonstrate this behaviour analytically for the

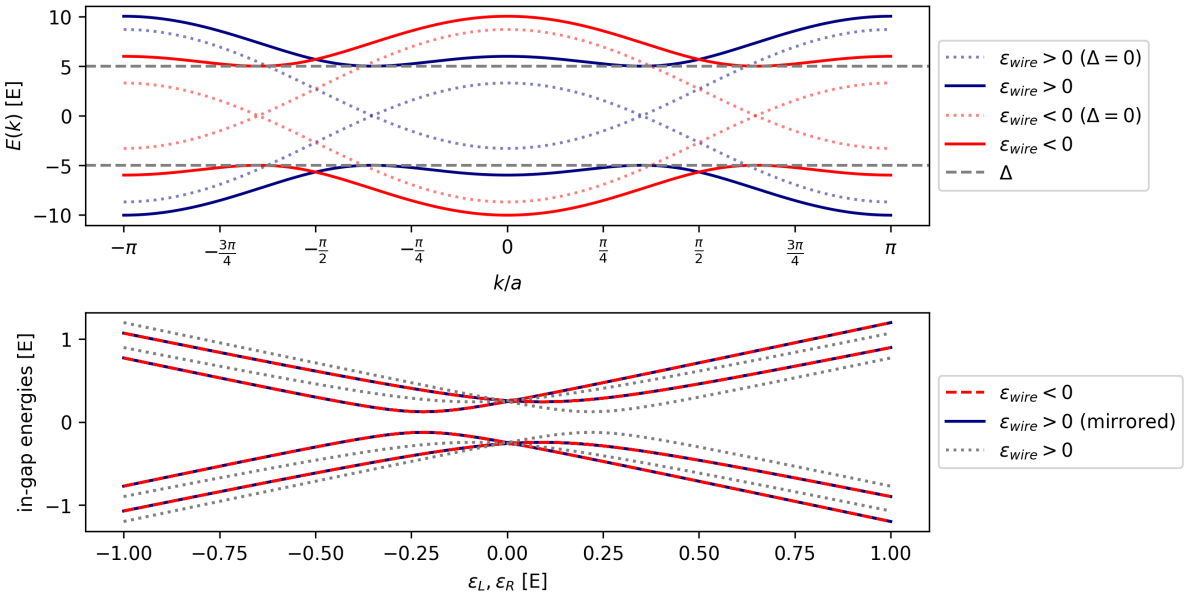

Figure 11: Top: Dispersion relation inside the 1D superconductor for the case with positive and negative on-site energy. The dispersion relation in the absence of superconductivity is also plotted for reference.
Bottom: In-gap eigenstates of the 1D dot-superconductor-dot model for positive and negative on-site energy in the superconductor. The positive on-site energy plot has also been mirrored around $\varepsilon_L, \varepsilon_R = 0$ to illustrate that it is identical to the negative energy one.

following simple 1D model: The left and right dots $|L\rangle, |R\rangle$ are represented as a single state each, and the superconductor is a continuous 1D system denoted $|x\rangle$ where $x \in (0, l_{SC})$. Since there is only a finite barrier between the dots and the superconductor, we make the following Ansatz for the wave function describing a particle on the left and right dots respectively:

$$|\psi_L\rangle = \alpha |L\rangle + \int \mathrm{d}x \frac{\beta}{\sqrt{N}} e^{ik_F x - x/\xi} |x\rangle + \gamma |R\rangle , \tag{110}$$

$$|\psi_R\rangle = \alpha |R\rangle + \int \mathrm{d}x \frac{\beta}{\sqrt{N}} e^{ik_F (l_{sc}-x) - (l_{sc}-x)/\xi} |x\rangle + \gamma |L\rangle . \tag{111}$$

Here, $N = \int_0^{l_{sc}} e^{-2x/\xi}$ is a normalization constant. α, β and γ are coefficients representing the relative weight of the wave-function in the dots and in the superconductor and k_F and ξ describe the fermi-wavevector and coherence length of the superconductor. These

two states can be combined into symmetric and anti-symmetric states:

$$|\psi_S\rangle := \frac{1}{\sqrt{2}}\left[|\psi_L\rangle + |\psi_R\rangle\right], \tag{112}$$

$$|\psi_A\rangle := \frac{1}{\sqrt{2}}\left[|\psi_L\rangle - |\psi_R\rangle\right]. \tag{113}$$

The weight of these wave functions in the superconductor is then the expectation value of the projection $P_{SC} = \int \mathrm{d}x\, |x\rangle\langle x|$. We find that:

$$\langle\psi_S \mid P_{SC} \mid \psi_S\rangle = 2\beta^2(1 + \frac{l_{SC}e^{-l_{SC}/\xi}}{N}\cos\left(k_F l_{sc}\right)), \tag{114}$$

$$\langle\psi_A \mid P_{SC} \mid \psi_A\rangle = 2\beta^2(1 - \frac{l_{SC}e^{-l_{SC}/\xi}}{N}\cos\left(k_F l_{sc}\right)). \tag{115}$$

This shows that for some values of the fermi-wavevector the symmetric state will have more weight within the superconductor while for other values of k_F the anti-symmetric state will have more weight.

7.1 Modeling a Minimal Kitaev Chain

The dot-superconductor-dot system has recently been discussed in great detail in the context of topological quantum computing and the search for Majorana bound states. For the Kitaev chain model [38], it has been theoretically predicted that Majorana bound states exist (quasi-particle fields γ_n, which are their own anti-particles, $\gamma_n^\dagger = \gamma_n$, anti-commute, $\{\gamma_n, \gamma_m\} = 2\delta_{nm}$ and are localized on the ends of the chain) for certain choices of the parameters defining the chain. The dot-superconductor-dot system resembles a minimal Kitaev chain with two sites, and for this system Majorana bound states have also been predicted [39] as well as experimentally observed [40]. These Majorana modes appear when the tunnel and CAR amplitudes are equal and the on-site dot energies are equal. They are robust towards fluctuations in the dot energies, but not towards noise which makes the tunnel and CAR amplitudes different. These Majorana bound states are therefore not topologically protected from noise in the same way as the Majorana bound states of the full Kitaev chain.

It is possible to study the relative magnitudes of the tunnel coupling t and the CAR coupling Δ by looking at the number parity of the ground state. In order to do so, we look at the system in a second-quantized framework (ignoring spin) where the basis $|00\rangle, |11\rangle, |10\rangle, |01\rangle$ denotes the number of particles in both the left and the right dot. The Hamiltonian in this basis is

$$H = \begin{pmatrix} 0 & \Delta & 0 & 0 \\ \Delta & \varepsilon_L + \varepsilon_R & 0 & 0 \\ 0 & 0 & \varepsilon_L & t \\ 0 & 0 & t & \varepsilon_R \end{pmatrix}. \tag{116}$$

The eigenvalues of this block diagonal matrix are readily determined to be:

$$E_{\text{even}} = \frac{\varepsilon_L + \varepsilon_R}{2} \pm \sqrt{\left(\frac{\varepsilon_L + \varepsilon_R}{2}\right)^2 + \Delta^2}, \tag{117}$$

$$E_{\text{odd}} = \frac{\varepsilon_L + \varepsilon_R}{2} \pm \sqrt{\left(\frac{\varepsilon_L - \varepsilon_R}{2}\right)^2 + t^2}. \tag{118}$$

The 'even' and 'odd' subscripts reference the number parity of the corresponding eigenstates. A phase diagram of this Hamiltonian as a function of the dot energies $\varepsilon_L, \varepsilon_R$ for different fixed values of t and Δ is given in Figure 12. The two phases are characterized by whether the ground state contains an even number of particles, (i.e. lives in the subspace spanned by $|00\rangle$ and $|11\rangle$) or contains an odd number of particles and is a superposition of $|01\rangle$ and $|10\rangle$.

We can establish the same phase diagram in the single-particle framework used in the finite element modeling of this system. Solving the finite element model for the in-gap states gives us eigenenergies of the system in relation to the chemical potential, so if these eigenenergies are negative, the state will be occupied. By the particle-hole symmetry of the BdG equations, there will always be the same number of eigenstates with energy above and below the chemical potential. On the black lines in Figure 12, which are the curves for which $\varepsilon_L \varepsilon_R = t^2 - \Delta^2$, an even-parity state and an odd-parity state are degenerate. This means that adding an extra particle costs zero energy, which in the single-particle picture means that there is an eigenstate crossing $E = 0$. We can therefore determine the phase transition in the single particle picture by looking for energy-level crossings at zero energy.

A crucial detail which we have glossed over in this discussion is the fact that we have ignored spin completely. In the presence of spin, but without magnetic fields, all energy levels are twofold degenerate due to Kramer's theorem [41]. This means that we can never have an odd-parity ground state as there will always be an even number of energy levels crossing zero. One possible way of breaking this degeneracy is by introducing a magnetic field. However, adding a magnetic field also affects the tunnel and CAR couplings, since the CAR couples states of opposite spin while the tunnel process couples states of the same spin. To overcome this, there must be spin-orbit interaction present in the system.[2] In Equation (109) we have included spin as well as SOI-induced CAR and tunnel couplings. We can project this Hamiltonian down to the subspace spanned by $|L\downarrow\rangle, |\overline{L\uparrow}\rangle, |R\downarrow\rangle, |\overline{R\uparrow}\rangle$,where L, R denotes the left and the right dots, $\uparrow, \downarrow$ denotes spin up and down relative to the magnetic field and $|\overline{L\uparrow}\rangle$ is the time-reversed counterpart of

[2]Or the superconductor must be a p-type superconductor pairing states of the same spin.

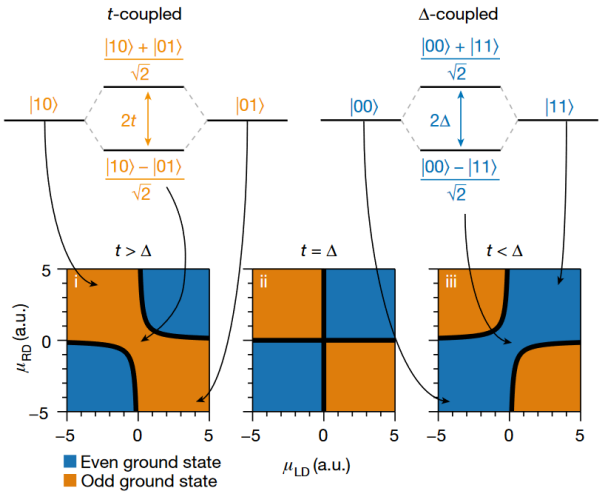

Figure 12: Phase diagram of the Hamiltonian Equation (116) for different values of the couplings. The chemical potentials in the two dots μ_{LD} and μ_{RD} effectively alter the dot energies ε_L and ε_R. From [40].

$|L\uparrow\rangle$. doing so, we get

$$\begin{pmatrix} \varepsilon_L - B & 0 & t & \Delta_{SO} \\ 0 & -\varepsilon_L + B & \Delta_{SO} & -t \\ t & -\Delta_{SO} & \varepsilon_R - B & 0 \\ \Delta_{SO} & -t & 0 & -\varepsilon_R + B \end{pmatrix}. \tag{119}$$

This matrix describes the same physics as the many-body Hamiltonian Equation (116), which we can see by comparing the phase diagram in Figure 12 with the eigenvalues of the matrix in Equation (119). By plotting the eigenvalue closest to zero for each value of the dot energies $\varepsilon_L, \varepsilon_R$ in 13 we can see that it approaches zero at the points where $(\varepsilon_L + B)(\varepsilon_R - B) = t^2 - \Delta_{SO}^2$. In fact, there are four subspaces of the full 8-dimensional Hilbert space, in which the Hamiltonian Equation (109) has the same structure as Equation (119). These four-dimensional subspaces are spanned by a spin-state and the time-reversal of the opposite spin-state on each dot. Each corresponding projected Hamiltonian therefore contains a SOI-induced coupling term as well as a regular coupling term. We can plot the smallest eigenvalue of the entire model Hamiltonian in eq. (109), in order to see how the relative strengths of all the coupling terms affect the location of the crossings at zero energy. In Figure 14 we have done so for different values of the SOI-induced coupling terms. The top left and bottom right regions of each of the 9 plots describe the crossing of opposite-spin states in the two dots and involve Δ and t_{SO} while the top right and bottom left regions of the plots describe the crossing of same-spin states and involve t and Δ_{SO}.

We have already seen that modifying the chemical potential in the superconductor

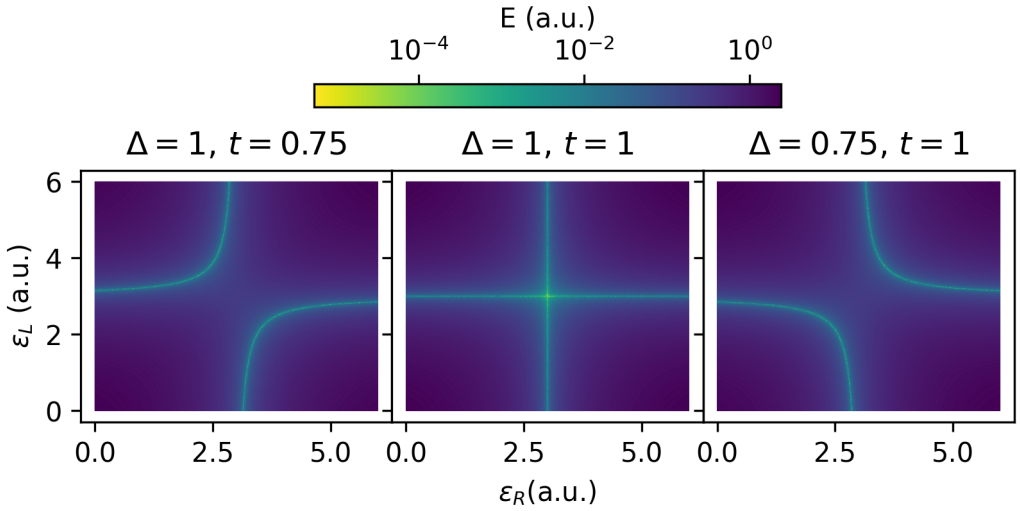

Figure 13: Smallest eigenvalue of the matrix in eq. (119) as a function of ε_L and ε_R for $B = 3(a.u.)$. All values are given in the same arbitrary unit scale. On the lines, there is a crossing of two eigenvalues at zero energy.

alters the tunnel and CAR couplings. For altering SOI-induced couplings, we argue that this can be achieved by altering the direction of the applied magnetic field, since the system is not planar symmetric. Based on this, we chose to study the lowest positive-energy eigenstate of the Finite element model as a function of the potential in the left and right dot for different chemical potentials in the superconductor and different directions of the magnetic field. Results of this are shown in Figure 15.

From this we observe that for some values of μ_{SC} the magnetic field direction indeed influences the coupling of the dots. For $\mu_{SC} = 3.48$ rotating the magnetic field from the x-direction to the y-direction appears to increase the difference $t^2 - \Delta_{SO}^2$ for the spin-up states (lower left region) while decreasing $t^2 - \Delta_{SO}^2$ for the spin-down states (top right region). Furthermore, it appears that for some of the parameters chosen, we are very close to the sweet-spot $t^2 = \Delta^2$. However, if we compare with Figure 9, we see that the apparent sweet-spots are likely due to the CAR coupling vanishing, so that we have uncoupled dots $t_{SO} = \Delta = 0$. This argument is further supported by the fact that for all of the parameter choices shown in Figure 15, the corresponding phase diagrams in Figure 14 suggest that the SOI-induced couplings are smaller than the regular ones.

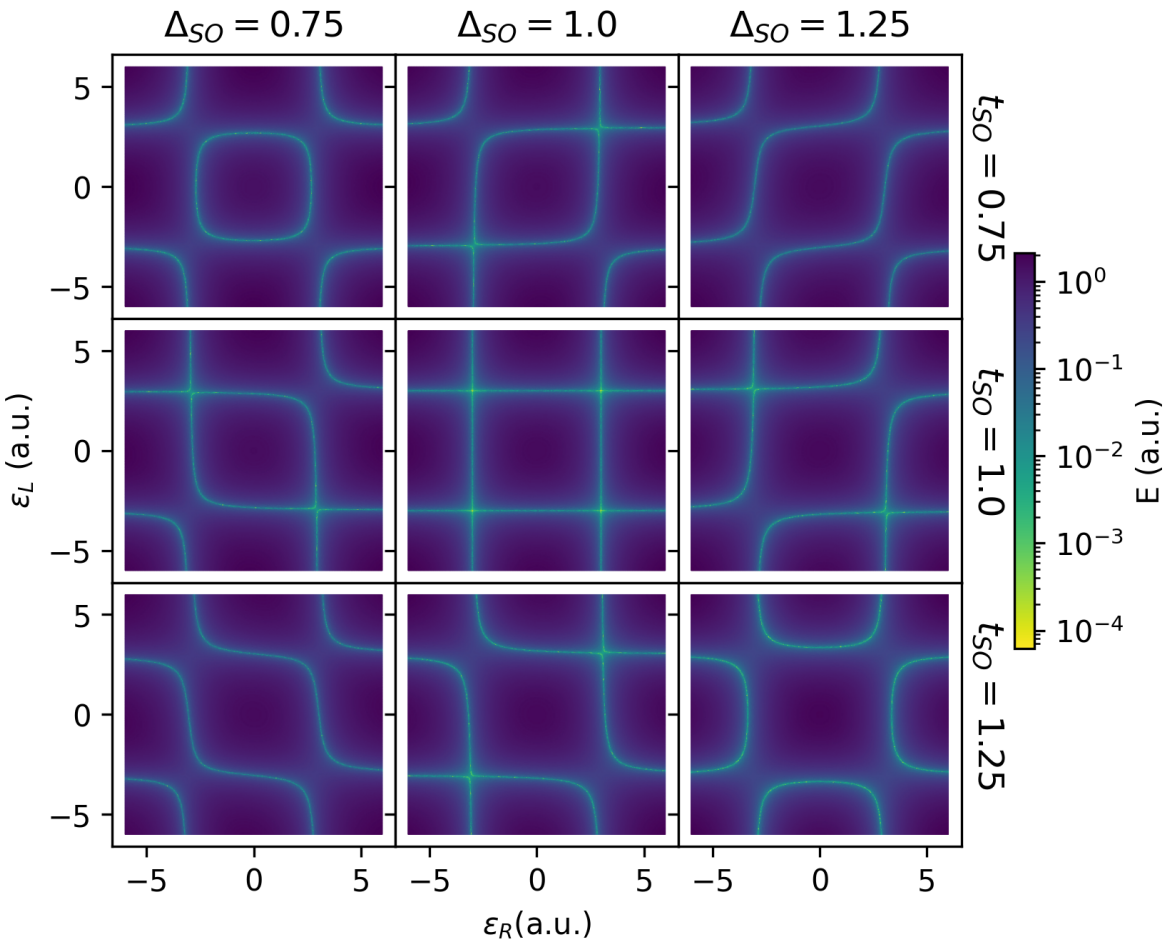

Figure 14: Smallest positive eigenvalue of Equation (109) as a function ε_L and ε_R for different values of the SOI-induced coupling coefficients t_{SO} and Δ_{SO}. For all of these, $B = 3(a.u.)$ and $t = \Delta = 1(a.u.)$. All values are given in the same arbitrary unit scale.

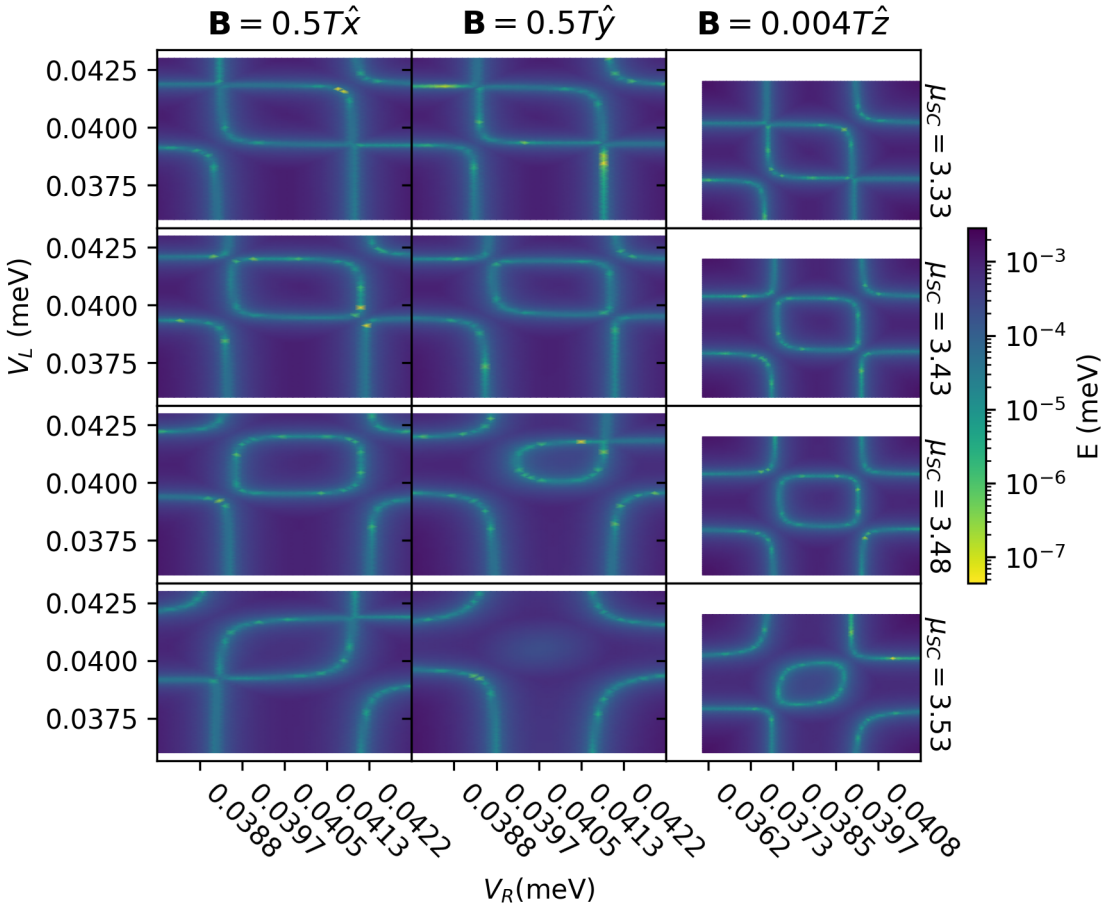

Figure 15: Lowest non-negative eigenvalue of the finite-element model as a function of the two dot potentials V_L and V_R. The chemical potential in the superconductor is expressed in meV. Note the different magnetic field magnitude in the z-direction compared to the in-plane directions, which was chosen as to get approximately the same splitting of the spin states.

8 Conclusions and Outlook

In this project, we set out with the intention of modeling spin-qubits in Germanium heterostructures in order to better understand these devices and how to design them. We have described how to construct a Hamiltonian which describes the dynamics of a single particle on a scale spanning multiple unit cells using the envelope-function approximation, and we have discussed the application of this method for describing heterostructures in the subband $k \cdot p$ method. We have also studied how Germanium, in contact with a superconductor, obtains an effective superconductive coupling due to the proximity effect and we have demonstrated how the nature of this coupling can be determined based on the model of the superconductor as well as the details of the tunneling process between superconductor and Germanium. In addition, we have reviewed the theory of invariants and how it can be used to obtain the Luttinger-Kohn Hamiltonian and we have directly used it to determine the form of the effective superconductive coupling in Germanium. With this Hamiltonian describing holes in Germanium heterostructures, we then showed how to solve the corresponding time-independent Schrödinger equation efficiently numerically using finite element methods to obtain the desired eigenstates of the Hamiltonian. Applying this approach to a simple model for a single spin-qubit, we showed that it is possible to choose an in-plane magnetic field direction in such a way that the qubit becomes robust towards gate-noise. Lastly, we studied a system consisting of two dots coupled via a superconductor. For this system we showed how to obtain parameters describing the tunneling and cross Andreev reflection couplings of the two dots, as well as demonstrated how one can use our approach in the search for device designs that are capable of hosting poor man's Majorana modes.

The analytical work of this project surrounding proximitized superconductivity in Section 3.1 and the determination of the superconductive parameter Δ using the theory of invariants in Section 4.2 raises an intriguing question about the compatibility of these two approaches. It would be interesting to study how the imposed symmetry constraint can be obeyed by a suitable description of the superconductor and the tunnel process between Germanium and superconductor. The methodology for modeling spin-qubit devices in Germanium developed in this project can readily be applied to the study of many phenomena not investigated here.

Interesting suggestions could for instance include **studying the effects of strain in Germanium devices**. The metallic contacts of the gates used to build the device cause strain in the Germanium material [42] and the spatial dependence of the strain can manipulate the spin [43]. It is therefore relevant to include strain in the model for it to accurately represent real devices. Using the theory of invariants, the strain tensor is readily added to the Luttinger-Kohn Hamiltonian (see e.g. [10]).

One could also look further into optimizing the **readout of singlet-triplet qubits**. Measuring the logical state of a singlet-triplet qubit uses Pauli spin-blockade which relies on the fact that two electrons (or holes) occupying the same quantum dot must be in a singlet state. Due to the differences in the shape of the quantum dots, however, the g-tensor varies from dot to dot, which causes the spins of different dots to split along different directions. The consequence of this is that it is possible for the two particles in a triplet state to tunnel occupy the same dot, since the spins of the particles are not exactly parallel. Using the model developed in this work, one could study ways of mitigating this phenomenon e.g. by picking the magnetic field direction cleverly.

Another interesting direction one could explore, would be to **increase the level of detail of the model** to better aid the design and development of Germanium devices. To achieve this, one could solve the electrostatics for the gates defining the system and use the resulting potential in place of the simple potential surfaces used in this project. Additionally, one could increase the accuracy of the model by extending the number of bands from 4 bands of the Luttinger-Kohn Hamiltonian to the 6, 8 or even 12 band Kane models. If modeling the z-direction as an infinite well is not accurate enough, one could also apply the subband $k \cdot p$ method for a different potential and basis set in the z-direction. The code used in this project can easily be extended to also model 3-dimensional systems, so it could also be used to study systems where we cannot assume that the motion of the z-direction decouples from the other two directions.

Lastly, one could look at how to **tune the Kitaev chain by altering the dot shapes**. Using the understanding of the effective g-tensor of the dots gained in Section 6, one could investigate if the dot-superconductor-dot system could be tuned to host poor man's Majorana states by altering the shapes of the quantum dots. Looking closer at the in-plane singular values in Figure 6 shows that for certain shapes of dots, the g-factor vanishes along one direction. Picking the two dots of the system to both have this shape but rotated 90° relative to each other, would, in the presence of a homogeneous global magnetic field, make the spins in the two dots align along orthogonal directions. For such a system, both CAR and tunnel processes would be possible without requiring SOI-induced spin-flipping during these processes. Initial numerical studies in this direction suggest that this approach may be promising.

References

[1] L. K. Grover. "A fast quantum mechanical algorithm for database search". en. In: *Proceedings of the twenty-eighth annual ACM symposium on Theory of computing - STOC '96*. Philadelphia, Pennsylvania, United States: ACM Press, 1996, pp. 212–219. DOI: 10.1145/237814.237866.

[2] P. Shor. "Algorithms for quantum computation: discrete logarithms and factoring". In: *Proceedings 35th Annual Symposium on Foundations of Computer Science*. Nov. 1994, pp. 124–134. DOI: 10.1109/SFCS.1994.365700.

[3] A. W. Harrow, A. Hassidim, and S. Lloyd. "Quantum Algorithm for Linear Systems of Equations". In: *Physical Review Letters* 103.15 (Oct. 2009). Publisher: American Physical Society, p. 150502. DOI: 10.1103/PhysRevLett.103.150502.

[4] J. Biamonte et al. "Quantum machine learning". en. In: *Nature* 549.7671 (Sept. 2017), pp. 195–202. DOI: 10.1038/nature23474.

[5] B. Cheng et al. "Noisy intermediate-scale quantum computers". en. In: *Frontiers of Physics* 18.2 (Apr. 2023), p. 21308. DOI: 10.1007/s11467-022-1249-z.

[6] G. Scappucci et al. "The germanium quantum information route". en. In: *Nature Reviews Materials* 6.10 (Oct. 2021). Number: 10, pp. 926–943. DOI: 10.1038/s41578-020-00262-z.

[7] N. W. Hendrickx et al. "Gate-controlled quantum dots and superconductivity in planar germanium". en. In: *Nature Communications* 9.1 (Dec. 2018). Number: 1, p. 2835. DOI: 10.1038/s41467-018-05299-x.

[8] M. Spethmann, S. Bosco, A. Hofmann, J. Klinovaja, and D. Loss. *High-fidelity two-qubit gates of hybrid superconducting-semiconducting singlet-triplet qubits*. en. arXiv:2304.05086 [cond-mat, physics:quant-ph]. Apr. 2023.

[9] M. Willatzen and L. C. Lew Yan Voon. *The k p Method*. en. Berlin, Heidelberg: Springer Berlin Heidelberg, 2009. DOI: 10.1007/978-3-540-92872-0.

[10] R. Winkler. *Spin-orbit coupling effects in two-dimensional electron and hole systems*. Springer tracts in modern physics v. 191. Berlin ; New York: Springer, 2003.

[11] A. Elçi and E. D. Jones. "Some consequences of the closure of the momentum Bloch functions". In: *Physical Review B* 34.12 (Dec. 1986). Publisher: American Physical Society, pp. 8611–8615. DOI: 10.1103/PhysRevB.34.8611.

[12] G. Bastard. "Superlattice band structure in the envelope-function approximation". In: *Physical Review B* 24.10 (Nov. 1981). Publisher: American Physical Society, pp. 5693–5697. DOI: 10.1103/PhysRevB.24.5693.

[13] M. G. Burt. "The justification for applying the effective-mass approximation to microstructures". en. In: *Journal of Physics: Condensed Matter* 4.32 (Aug. 1992), p. 6651. DOI: 10.1088/0953-8984/4/32/003.

[14] J.-X. Zhu. *Bogoliubov-de Gennes Method and Its Applications*. en. Vol. 924. Lecture Notes in Physics. Cham: Springer International Publishing, 2016. DOI: 10.1007/978-3-319-31314-6.

[15] P. G. De Gennes. *Superconductivity of Metals and Alloys*. en. 1st ed. CRC Press, Mar. 2018. DOI: 10.1201/9780429497032.

[16] M. Tinkham. *Introduction to superconductivity*. eng. 2 ed. Dover books on physics. Mineola, NY: Dover Publ, 2015.

[17] K. Aggarwal et al. "Enhancement of proximity-induced superconductivity in a planar Ge hole gas". In: *Physical Review Research* 3.2 (Apr. 2021). Publisher: American Physical Society, p. L022005. DOI: 10.1103/PhysRevResearch.3.L022005.

[18] A. Tosato et al. "Hard superconducting gap in germanium". In: *Communications Materials* 4.1 (Apr. 2023). arXiv:2206.00569 [cond-mat], p. 23. DOI: 10.1038/s43246-023-00351-w.

[19] J. Danon. *Interaction effects on the pairing potential in a nanowire*. Mar. 2017.

[20] T. D. Stanescu, R. M. Lutchyn, and S. Das Sarma. "Majorana fermions in semiconductor nanowires". In: *Physical Review B* 84.14 (Oct. 2011). Publisher: American Physical Society, p. 144522. DOI: 10.1103/PhysRevB.84.144522.

[21] H. Bruus and K. Flensberg. *Many-body quantum theory in condensed matter physics: an introduction*. Oxford graduate texts. OCLC: ocm56694794. Oxford ; New York: Oxford University Press, 2004.

[22] G. L. Bir and G. E. Pikus. *Symmetry and strain-induced effects in semiconductors*. engrus. New York: Wiley, 1974.

[23] B. Simon. *Representations of finite and compact groups*. Graduate studies in mathematics v. 10. Providence, R.I: American Mathematical Society, 1996.

[24] G. Koster, J. Dimmock, R. Wheeler, and H. Statz. *Properties of the thirty-two point groups*. M.I.T. press research monographs. tex.lccn: 63021194. M.I.T. Press, 1963.

[25] M. G. Larson and F. Bengzon. *The Finite Element Method: Theory, Implementation, and Applications*. en. Vol. 10. Texts in Computational Science and Engineering. Berlin, Heidelberg: Springer, 2013. DOI: 10.1007/978-3-642-33287-6.

[26] L. C. Evans. *Partial differential equations*. eng. Second edition. Graduate studies in mathematics 19. Providence, Rhode Island: American Mathematical Society, 2022.

[27] M. W. Scroggs, I. A. Baratta, C. N. Richardson, and G. N. Wells. "Basix: a runtime finite element basis evaluation library". en. In: *Journal of Open Source Software* 7.73 (May 2022), p. 3982. DOI: 10.21105/joss.03982.

[28] *Unified form language: A domain-specific language for weak formulations of partial differential equations: ACM Transactions on Mathematical Software: Vol 40, No 2.*

[29] M. W. Scroggs, J. S. Dokken, C. N. Richardson, and G. N. Wells. "Construction of Arbitrary Order Finite Element Degree-of-Freedom Maps on Polygonal and Polyhedral Cell Meshes". In: *ACM Transactions on Mathematical Software* 48.2 (2022), 18:1–18:23. DOI: 10.1145/3524456.

[30] J. E. Roman and A. Tomas. "Krylov-Schur Methods in SLEPc". en. In: ().

[31] V. Hernandez, J. E. Roman, and V. Vidal. "SLEPc: A scalable and flexible toolkit for the solution of eigenvalue problems". In: *ACM Transactions on Mathematical Software* 31.3 (Sept. 2005), pp. 351–362. DOI: 10.1145/1089014.1089019.

[32] S. Balay et al. *PETSc/TAO Users Manual*.

[33] L. D. Dalcin, R. R. Paz, P. A. Kler, and A. Cosimo. "Parallel distributed computing using Python". en. In: *Advances in Water Resources*. New Computational Methods and Software Tools 34.9 (Sept. 2011), pp. 1124–1139. DOI: 10.1016/j.advwatres.2011.04.013.

[34] L. Chirolli and G. Burkard. "Decoherence in Solid State Qubits". In: *Advances in Physics* 57.3 (May 2008). Number: 3 arXiv:0809.4716 [cond-mat, physics:quant-ph], pp. 225–285. DOI: 10.1080/00018730802218067.

[35] G. Ithier et al. "Decoherence in a superconducting quantum bit circuit". en. In: *Physical Review B* 72.13 (Oct. 2005). Number: 13, p. 134519. DOI: 10.1103/PhysRevB.72.134519.

[36] K. Kraus and A. Bohm. *States, effects, and operations: fundamental notions of quantum theory ; lectures in mathematical physics at the University of Texas at Austin*. en. Lecture notes in physics 190. Berlin Heidelberg: Springer, 1983.

[37] B. Venitucci, L. Bourdet, D. Pouzada, and Y.-M. Niquet. "Electrical manipulation of semiconductor spin qubits within the g-matrix formalism". In: *Physical Review B* 98.15 (Oct. 2018). Number: 15 Publisher: American Physical Society, p. 155319. DOI: 10.1103/PhysRevB.98.155319.

[38] A. Y. Kitaev. "Unpaired Majorana fermions in quantum wires". en. In: *Physics-Uspekhi* 44.10S (Oct. 2001), p. 131. DOI: 10.1070/1063-7869/44/10S/S29.

[39] M. Leijnse and K. Flensberg. "Parity qubits and poor man's Majorana bound states in double quantum dots". In: *Physical Review B* 86.13 (Oct. 2012). arXiv:1207.4299 [cond-mat, physics:quant-ph], p. 134528. DOI: 10.1103/PhysRevB.86.134528.

[40] T. Dvir et al. "Realization of a minimal Kitaev chain in coupled quantum dots". en. In: *Nature* 614.7948 (Feb. 2023). Number: 7948 Publisher: Nature Publishing Group, pp. 445–450. DOI: 10.1038/s41586-022-05585-1.

[41] J. J. Sakurai and J. Napolitano. *Modern quantum mechanics*. eng. 3rd ed. Cambridge: Cambridge University Press, 2021.

[42] C. Corley-Wiciak et al. "Nanoscale Mapping of the 3D Strain Tensor in a Germanium Quantum Well Hosting a Functional Spin Qubit Device". In: *ACS Applied Materials & Interfaces* 15.2 (Jan. 2023). Publisher: American Chemical Society, pp. 3119–3130. DOI: 10.1021/acsami.2c17395.

[43] J. C. Abadillo-Uriel, E. A. Rodríguez-Mena, B. Martinez, and Y.-M. Niquet. *Hole spin driving by strain-induced spin-orbit interactions*. arXiv:2212.03691 [cond-mat]. Dec. 2022. DOI: 10.48550/arXiv.2212.03691.